JOURNAL OF GEOPHYSICAL RESEARCH, VOL. 115, C02003, doi:10.1029/2009JC005360, 2010

Transient upwelling hot spots in the oligotrophic North Pacific

P. H. R. Calil[1] and K. J. Richards[1,2]

Received 6 March 2009; revised 7 September 2009; accepted 18 September 2009; published 3 February 2010.

[1] Vertical exchange between deep, nutrient-rich and nutrient-depleted surface waters controls the physical supply of nutrients into the euphotic zone in the oligotrophic waters of the subtropical North Pacific Ocean. Sea surface temperature and ocean color satellite images are used in this study to show that submesoscale chlorophyll patches are locally intensified. These patches are associated with surface temperature fronts and regions of strong stretching of the eddying flow. The latter are identified by calculating the finite-size Lyapunov exponents of the geostrophic flow derived from the sea surface height field from altimetry. Surface frontogenesis and nonlinear Ekman pumping (NLEP) arise as natural candidates for the sporadic generation of large vertical velocities that could favor the formation of these features. A high-resolution regional numerical model simulation confirms that large vertical velocities are indeed associated with strong density fronts and gradients of relative vorticity. Using the Q vector divergence as a proxy for frontogenetically generated vertical velocities yields good agreement with the model vertical velocities, particularly in regions where they are large. The pattern and magnitude of NLEP suggests that it is also contributing to the strong vertical motions, although NLEP and model vertical velocities are not necessarily in phase. Surface frontogenesis and NLEP provide a possible explanation for the episodic injection of nutrients at the submesoscale, which are then horizontally stirred and modulated by the unstable manifolds of the flow field. Given that these surface-intensified processes would be biogeochemically more effective when the pycnocline is shallow, they could also serve as one possible explanation for the late summer chlorophyll blooms that are known to occur in the region.

Citation: Calil, P. H. R., and K. J. Richards (2010), Transient upwelling hot spots in the oligotrophic North Pacific, *J. Geophys. Res.*, *115*, C02003, doi:10.1029/2009JC005360.

1. Introduction

[2] The central portion of the oceanic subtropical gyres is usually referred to as an ocean desert. Export production estimates in these regions, although modest, account for roughly half of the global export of organic carbon to the interior because of the areal extent of the subtropical gyres [*Williams and Follows*, 2003]. This raises the long-standing question about the processes that bring nutrients into the euphotic zone in the oligotrophic ocean to support the estimated levels of export production and phytoplankton growth [*Martin and Pondaven*, 2003; *Oschlies*, 2002; *McGillicuddy and Robinson*, 1997].

[3] One of these processes is the eddy-pumping mechanism [*McGillicuddy et al.*, 1998; *McGillicuddy and Robinson*, 1997; *Falkowski et al.*, 1991]. At mesoscales, the uplift of isopycnals, which occurs at the center of cyclones and at the edges of anticyclones, primarily in their formation stages, bring nutrient-rich waters into the euphotic zone. Because of the vertical asymmetry in the light field, uplifted isopycnals would have an ecosystem impact and cause a net upward flux of nutrients [*McGillicuddy and Robinson*, 1997]. Other mesoscale processes include the so called "eddy-wind interaction." The divergence of the Ekman transport within the horizontal scale of an eddy generates small, but persistent vertical velocities [*McGillicuddy et al.*, 2007; *Martin and Richards*, 2001].

[4] The interaction between mesoscale vortices, ubiquitous in the surface ocean, creates regions of large straining that induce, in many cases, an enhancement of surface, horizontal density gradients which leads to the disruption of the thermal wind balance, a process known as frontogenesis [*Hoskins and Bretherton*, 1972]. Ageostrophic secondary circulation (ASC) cells are then generated in a plane perpendicular to the density front in order to restore the balance [*Lapeyre and Klein*, 2006; *Hoskins*, 1982]. In such regions the Rossby number, Ro ($Ro = \frac{\xi}{f}$, where ξ is the vertical component of the relative vorticity and f is the planetary vorticity), is O(1) and nonlinear Ekman pumping (NLEP), a consequence of the advection of the surface geostrophic vorticity by the Ekman flow, also becomes important, potentially generating large vertical velocities [*Mahadevan et al.*, 2008; *Mahadevan and Tandon*, 2006; *Thomas and Rhines*, 2002]. The relative importance of some of the processes described above (e.g., eddy wind

[1]Department of Oceanography, University of Hawaii at Manoa, Honolulu, Hawaii, USA.
[2]International Pacific Research Center, University of Hawaii at Manoa, Honolulu, Hawaii, USA.

0148-0227/10/2009JC005360$09.00

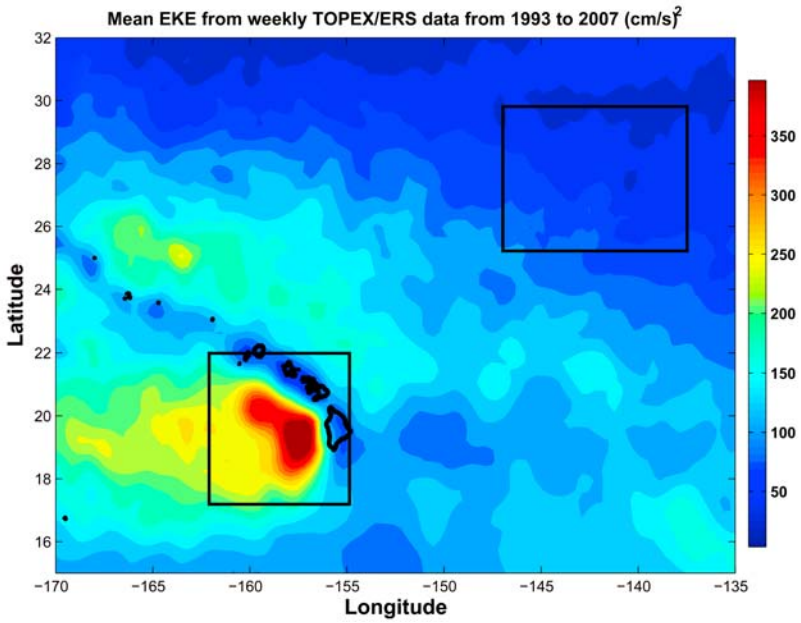

Figure 1. Average EKE calculated from SSH anomaly for the period between 1993 and 2007. The boxes outline the two regions used in the observational examples.

versus NLEP) is currently the subject of debate [cf. *Mahadevan et al.*, 2008; *McGillicuddy et al.*, 2008, 2007].

[5] In this study, we use remotely sensed data which suggest that chlorophyll-a patches in the oligotrophic ocean around Hawaii are intensified at submesoscales. These patches are shown to be also associated with weak temperature fronts. Because of the lack of subsurface data, high-resolution model simulations are used to illustrate the vertical structure of the ocean within regions of large straining. Frontogenesis and NLEP are calculated and compared with modeled vertical velocities. Linked with horizontal stirring, these mechanisms could help explain the streaky chlorophyll-a pattern observed in the region, with implications for primary and export production.

[6] This paper is organized as follows. In section 2, two examples of observed filamental chlorophyll-a structures associated with temperature fronts, possibly enhanced by temperature advection caused by the mesoscale eddies, are shown in the following two distinct regions: (1) the lee of the islands, with strong mesoscale eddies, and (2) the region northeast of the island chain, where weaker mesoscale eddies are also shown to be important agents in creating regions of large straining where large vertical velocities can be locally generated. Given the regional characteristics, two processes, surface frontogenesis and NLEP, are indicated as the most relevant in generating transient, large vertical velocities at the base of the mixed layer and, hence, potentially responsible for submesoscale nutrient injections which are subsequently horizontally distributed. In section 3, geostrophic velocities from satellite altimetry are used to identify the unstable manifolds and relate them with the observed chlorophyll-a and temperature images. In section 4, we perform high-resolution 3-D model simulations and show that surface frontogenesis and NLEP, particularly the former in this case, are indeed active around regions of strong gradient in surface relative vorticity and surface density gradients, where vertical velocities are large. Discussion and concluding remarks are given in section 5.

2. Observations

[7] In order to demonstrate the general validity of our results, we are going to explore observations of meso- and submesoscale chlorophyll-a patches in regions around Hawaii within the following two different dynamical regimes (see Figure 1): (1) the highly energetic lee of the islands, characterized by strong mesoscale eddies and robust wind forcing [*Calil et al.*, 2008; *Kuwahara et al.*, 2008; *Nencioli et al.*, 2008; *Lumpkin*, 1998], and (2) the region northeast of the islands, with low EKE and weaker mesoscale eddies generated by intrinsic instabilities of the geostrophic flow. The latter region is also characterized by late summer chlorophyll-a blooms [*Dore et al.*, 2008; *Wilson*, 2003]. The cause of such blooms is beyond the scope of this paper, but the processes described below can serve as an explanation for the episodic injection of nutrients at submesoscales, which might be facilitated at different times of the year.

[8] Sea surface temperature (SST) and chlorophyll-a data used in this section were obtained from 8 day averages of the Moderate Resolution Imaging Spectroradiometer (MODIS) at 4 km resolution. Surface chlorophyll-a concentration in this region is representative over one attenuation length, which at Station ALOHA is, approximately, 23 m (R. R. Bidigare, personal communication, 2009). Sea surface height (SSH) anomaly data were obtained from the AVISO merged product of TOPEX Poseidon, ERS and Jason-1 satellites at approximately 30 km resolution. The altimeter products were produced by the CLS Space Oceanography Division as part of the Environment and Climate EU ENACT project (EVK2-CT2001-00117) and with support from the Centre National d'Etudes Spatiales (CNES).

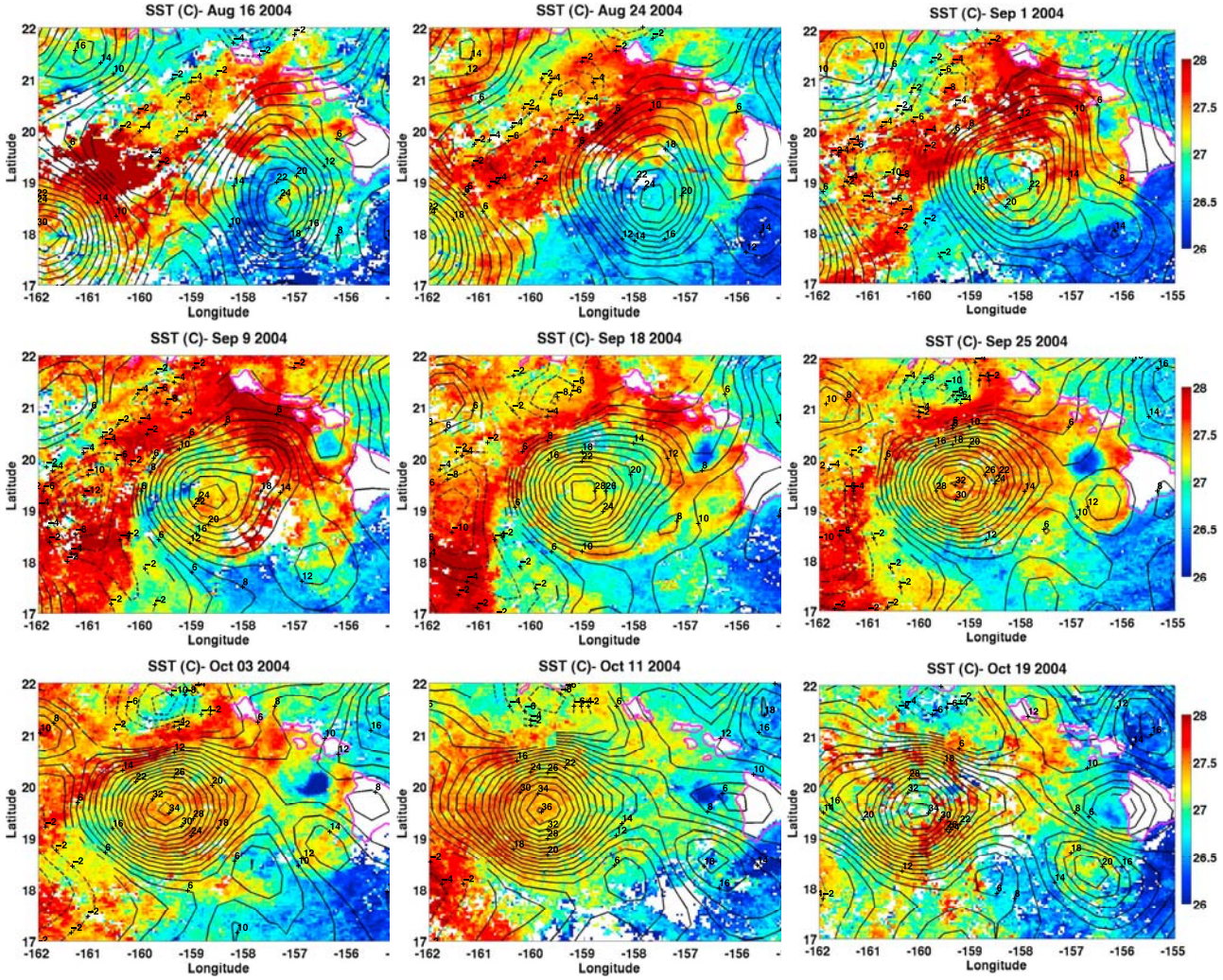

Figure 2. SST (color) and SSH anomaly, with thick (dashed) contours representing negative(positive) values (cm) in the lee of the Hawaiian islands from 8 August to 19 October 2004 (data source is MODIS).

2.1. Lee of the Islands

[9] The formation and evolution of a chlorophyll-a filament associated with the edges of an anticyclonic eddy in the lee of the islands can be seen from SST and surface chlorophyll-a images from 8 August to 19 October 2004, shown in Figures 2 and 3.

[10] The anticyclonic eddy is typical of the lee eddies formed just southwest off the island of Hawaii. Roughly circular, with a diameter of approximately 150 km, it was formed at the end of July 2004, propagated westward with a translation speed of approximately 0.05 m s^{-1} and its signal as a coherent structure can be detected for, approximately, 26 weeks. In its initial stages, it intensifies and reaches a maximum amplitude, as detected by the SSH anomaly, on 11 October 2004. After that it propagates west-southwestward, following a very similar pattern to anticyclonic eddies previously studied [*Calil et al.*, 2008; *Flament et al.*, 2001].

[11] From the SST images (Figure 2), we can see that the anticyclone modulates the exchange of the warm Hawaiian Lee Countercurrent (HLCC) waters flowing from the west with the colder waters from the east that are advected into the region by the northern branch of the North Equatorial Current (NEC). The edges of the anticyclone are regions where stretching deformation is largest. One of the consequences of large stretching is the advection of the temperature field in such a way that the isotherms are condensed along the axis of dilatation. In other words, the initial horizontal temperature gradient is enhanced by the action of the eddy.

[12] When it comes to the evolution of the surface chlorophyll-a field (Figure 3), the effect of the eddy is to initially trap a large chlorophyll-a patch in its center. The chorophyll a concentration, although very low (≈0.05 mg m^{-3}), is larger than the surroundings. However, there is no increase in values in this two week period.

[13] Noticeable increases in chlorophyll-a concentration can be seen from 17 September 2004 onward at the edges of the anticyclone, particularly on its northwestern limb, where the horizontal temperature gradient is large. Subsequently, a consistent ring-like structure, coincident with the edges of the anticyclone, is seen with values of, approximately, 0.1 mg m^{-3}.

[14] The sequence of images suggest that the patch is intensified by local mechanisms rather than horizontal accumulation, since there is no patch with high chloro-

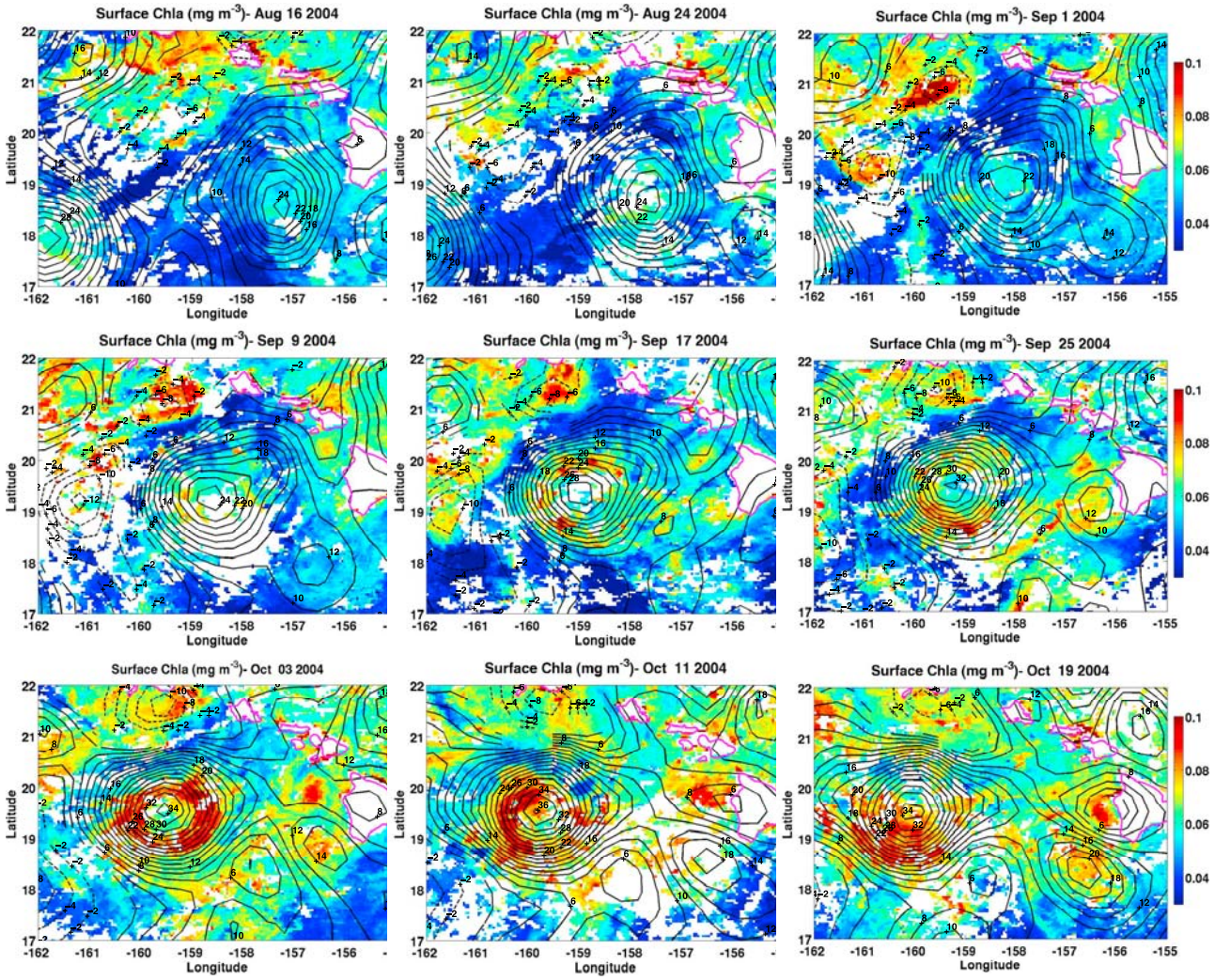

Figure 3. Surface chorophyll-a concentration (color) and SSH anomaly, with thick (dashed) contours representing negative (positive) values (cm) in the lee of the Hawaiian islands from 8 August to 19 October 2004 (data source is MODIS).

phyll-a concentrations in the surroundings, and the ring-like structure is confined to the edges of the anticyclone. This makes the possibility of vertical injection of nutrients prompting a bloom plausible, with the horizontal stirring concomitantly acting to spread the filament.

[15] Once the eddy starts decaying, the ring-like chlorophyll-a patch is dispersed horizontally, being no longer confined by the edges, and the chlorophyll-a concentration starts to decrease. The horizontal temperature gradients are simultaneously reduced.

2.2. Northeastern Region

[16] Another example of the filamentation process and possible submesoscale, local, episodic injections associated with eddies and surface temperature fronts is shown in Figures 4 and 5, for SST and chlorophyll-a, respectively, in the region to the northeast of the Hawaiian islands, from 31 July to 9 September 2004. This is a region of low EKE and weak mesoscale eddies subjected to the strong trade winds, which are more intense during summer months.

[17] Looking first at chlorophyll-a (Figure 5), the intensification of the filament occurs at smaller scales and, as in the previous example, does not appear to be a consequence of horizontal accumulation, as the filamental structure seems stable and independent of the surrounding region. The persistence and intensification of the patches over three weeks require local mechanisms of vertical injection, since there is no other source of nutrients in this oligotrophic region.

[18] From the initial development of the chorophyll patch (when concentrations were very low and no structure was discernible), to 24 August 2004 (when the chlorophyll-a filament is most distinguishable), it is clear that the intensification is closely associated with the edges of the strongest (as estimated by the SSH maximum) anticyclone, centered near 143°W, as well as with straining regions between weaker vortices (mostly weak anticyclones) to the east.

[19] A notable feature of this filamentary structure (particularly the structure centered at about 139°W, but also

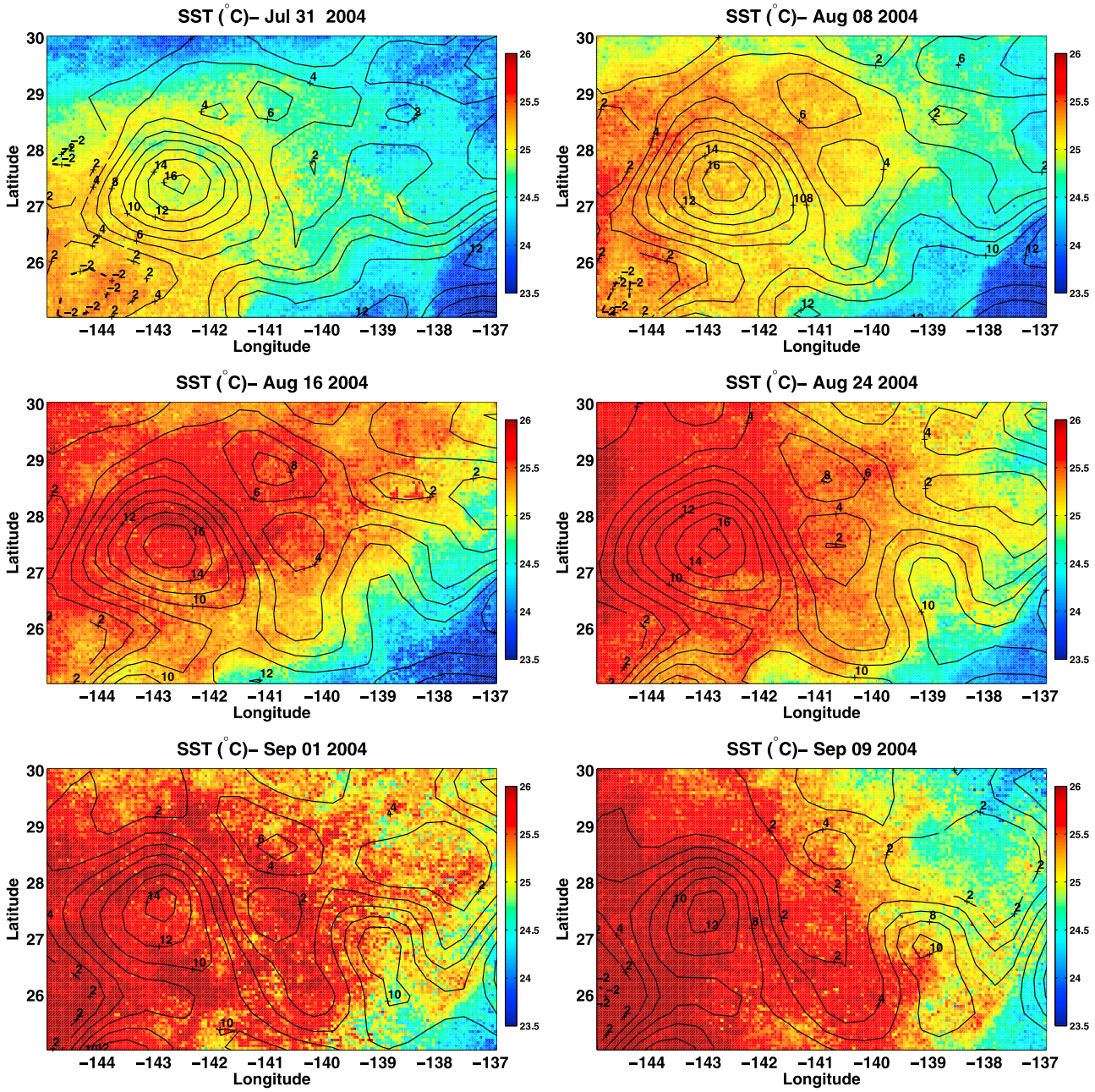

Figure 4. SST for the northeastern region from 31 July to 9 September 9 2004 (data source is MODIS).

distinguishable in the anticyclone further to the west) is that it appears to be closely related to warm SST anomalies imposed by the stretching geostrophic flow, as seen in Figure 4, on 24 August 2004. A point-by-point correlation yielded very low values, making it difficult to draw a quantitative conclusion about the relationship between SST and chlorophyll-a. The visual correspondence suggests, however, that warm anomalies are associated with larger chlorophyll-a concentrations, a picture consistent with surface frontogenesis [*Legal et al.*, 2007; *Hakim et al.*, 2002].

[20] An important characteristic of this region is the persistent northeasterly trade winds. In the example of Figures 4 and 5, the winds are aligned with the main temperature front. Down front winds will generate Ekman transport of denser waters from the southeast over lighter waters in the northwest [*Thomas and Lee*, 2005]. Such conditions would be favorable to convective mixing and frontogenesis, from which vertical motion would ensue.

3. Finite-Size Lyapunov Exponents

[21] From the examples in the previous section, it seems likely that the chlorophyll-a patches are associated with surface temperature fronts and regions of large straining in the vicinity of mesoscale features. These regions are characterized by large horizontal shear and strain deformation, large relative vorticity and, consequently, O(1) Rossby number.

[22] Frontogenesis is the intensification of fronts as a consequence of deformation and/or convergence of the

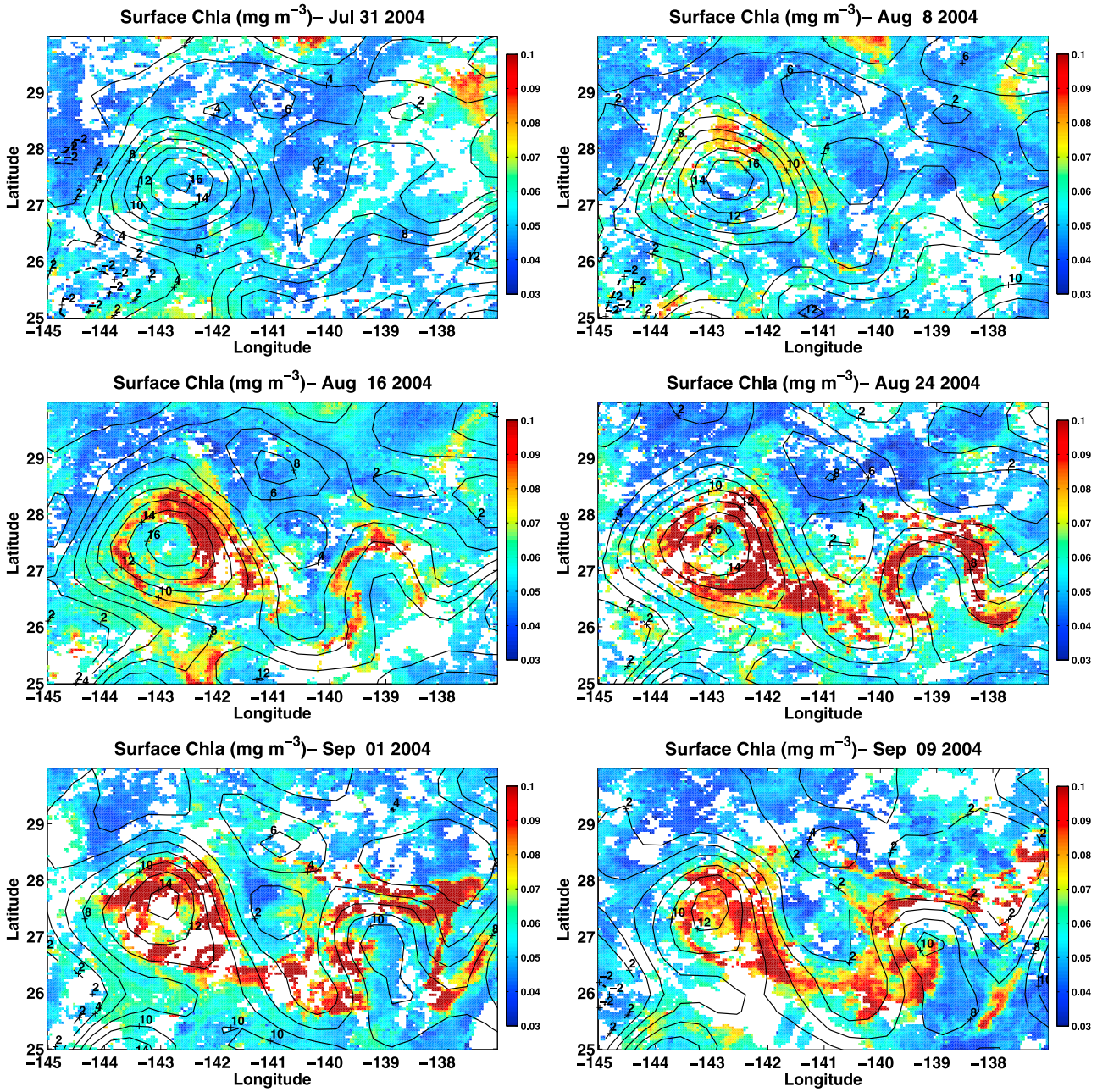

Figure 5. Surface chlorophyll-a concentration to the northeast of the Hawaiian islands from 31 July to 9 September 2004 (data source is MODIS).

flow. The imbalance in geostrophy created by the enhancement of the horizontal density gradients gives rise to ageostrophic, counterrotating cells that act to reestablish the balance, with downwelling on the cold side of the front and upwelling on the warm side of the front [*Hakim et al.*, 2002; *Lapeyre and Klein*, 2006; *Legal et al.*, 2007]. This can also be understood in terms of conservation of potential vorticity, where an accelerating jet (e.g., a region of large straining in between two mesoscale eddies) will generate downwelling on the cyclonic side of the frontal region and upwelling on the anticyclonic side, due to stretching and squeezing, respectively, of the thickness of the isopycnal layer [*Pollard and Regier*, 1992].

[23] In a slowly evolving, pure strain velocity field, frontogenesis will primarily occur along the axis of dilatation while frontolysis will occur along the axis of contraction. In an Eulerian reference frame, these are the regions of large deformation (i.e., strain-dominated regions). However, frontogenesis will only be effective if water parcels remain for enough time within a frontogenetical region. Lagrangian diagnostics provide a useful tool for identifying frontogenetically active regions.

[24] An effective way to diagnose regions of large stretching, prone to frontogenesis, is to compute the finite-size Lyapunov exponent (FSLE), which corresponds to the inverse time scale of the separation of adjacent pairs of parcels initially separated infinitesimally [*d'Ovidio et al.*,

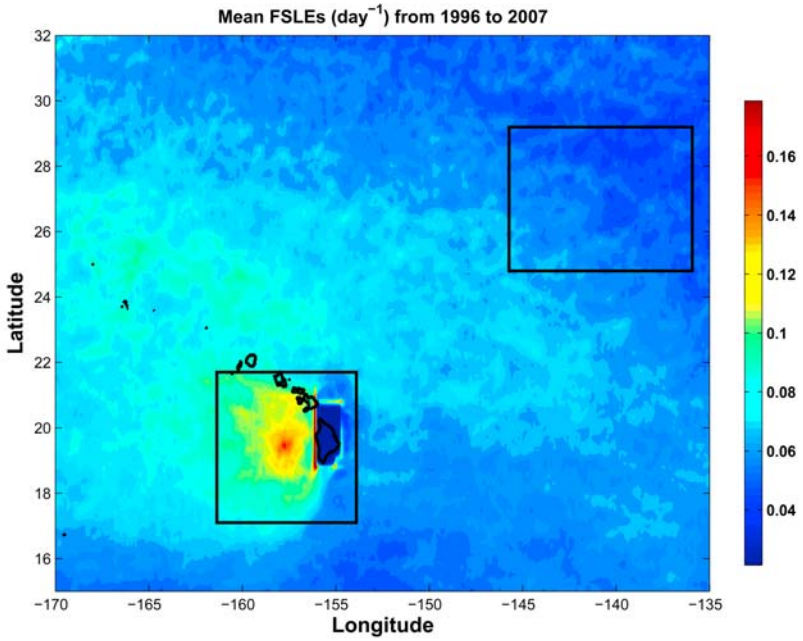

Figure 6. Average FSLEs calculated from surface geostrophic velocities from 1998 to 2006. The boxes outline the two regions studies as in Figure 1.

2004; *Artale et al.*, 1997; *Aurell et al.*, 1997]. The FSLE is defined as

$$\lambda = \frac{1}{\tau} \log \frac{\delta_f}{\delta_0}, \tag{1}$$

where τ is the time taken by the two trajectories, initially separated by a distance δ_0, in our case 0.01°, to reach the final distance δ_f, in our case 50 km, which is approximately the Rossby radius of deformation in the region. In this section, the velocity field used to calculate the FSLE is obtained from 8 day averaged absolute geostrophic velocities from the merged AVISO altimetry data set. A bilinear interpolation assigns velocities to grid points below the resolution of the altimetry data set. The chaotic evolution of the mesoscale eddy field generates structures at smaller scales than that of the velocity product. In other words, relatively course velocity fields can produce filamentation of tracers down to much smaller scales than those of the flow field itself. The same is true for the FLSE field. It is of note that the finer grid is not to a get a better representation of the flow field but to resolve the fine structures produced by it. For example, a pure strain flow, with no diffusion, will stretch out a tracer to become infinitesimally thin. Lagrangian detection of transport barriers has been shown to capture such structures [*Lehahn et al.*, 2007].

[25] The FSLE is obtained by calculating the separation of initially nearby particles as time moves forward or backward. When this separation reaches the final length scale(δ_f) the integration is stopped and the inverse time is mapped onto the geographic coordinates of the initial position. In our case, the velocity field is integrated backward in time in order to detect the unstable manifolds of the flow field.

[26] Regions with the largest backward FSLE, a proxy for the unstable manifolds of the flow field, are the regions where the particle pair separation is maximum and can be understood as the Lagrangian dilatation axis of the flow, along which transport will occur. If, on the other hand, particles are located within regions where separation is small (e.g., particles trapped by mesoscale eddies or in regions of very weak currents) the time required to reach the final distance will be large and the backward FSLE value will be low.

[27] The FSLE also allow us to infer characteristics of the transport of passive tracers, since unstable manifolds act as transport barriers across which the transport of tracers is restricted. It has also been hypothesized that the unstable manifolds are related to frontogenetically generated vertical velocities [*Lehahn et al.*, 2007]. The reader is referred to *d'Ovidio et al.* [2004] for details of the technique.

3.1. Averaged Values

[28] The spatial structure of horizontal stirring in the ocean is not uniform [*Waugh and Abraham*, 2008]. An accurate idea of its regional pattern can be obtained by calculating the average of weekly FSLE's for the same region shown in Figure 1 for the period between 1998 and 2007. Figure 6 shows that the two outlined regions have, as in the case of EKE, distinct dynamical characteristics, with the lee of the islands as a region of much more vigorous horizontal stirring and EKE.

[29] Previous studies have observed a relationship between averaged finite-time Lyapunov exponents, where particles are advected for a given time, as opposed to the FSLE where the distance determines the time of integration, and EKE [*Waugh et al.*, 2006; *Waugh and Abraham*, 2008] and suggested that regions of large stirring and EKE would also affect the distribution of tracers. Our results confirm a

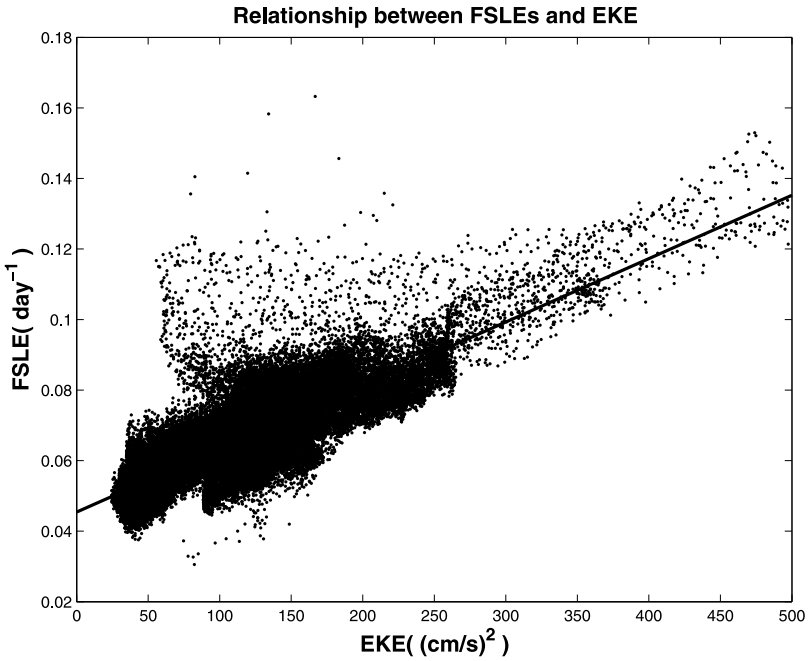

Figure 7. Scatterplot of averages of FSLEs and EKE. The correlation coefficient between the two is 0.79.

relationship between annually averaged EKE and FSLE in the vicinity of the Hawaiian islands. In our case a linear fit is a good approximation for the relationship between EKE and FSLE's (Figure 7). The point-by-point correlation coefficient between the averaged values is 0.79, which is significant at the 95% level of confidence. It is of note, however, that the large correlation might hold only for this limited region, particularly the lee of the islands, with the frequent shedding of coherent structures. *d'Ovidio et al.* [2009] suggest that averaged FSLE and EKE do not necessarily provide the same information about the flow field.

[30] The surface chlorophyll-a average for the region did not have a clear relationship with FSLE or EKE. Noting the meridional gradient that exists in the average values (with higher values to the north), we detrended the average values meridionally by removing a linear fit at each longitude (the average slope was, approximately, 0.02 kg m^{-3} km^{-1}). The result is shown in Figure 8. The correlation coefficients between the detrended chlorophyll-a average and FSLE is

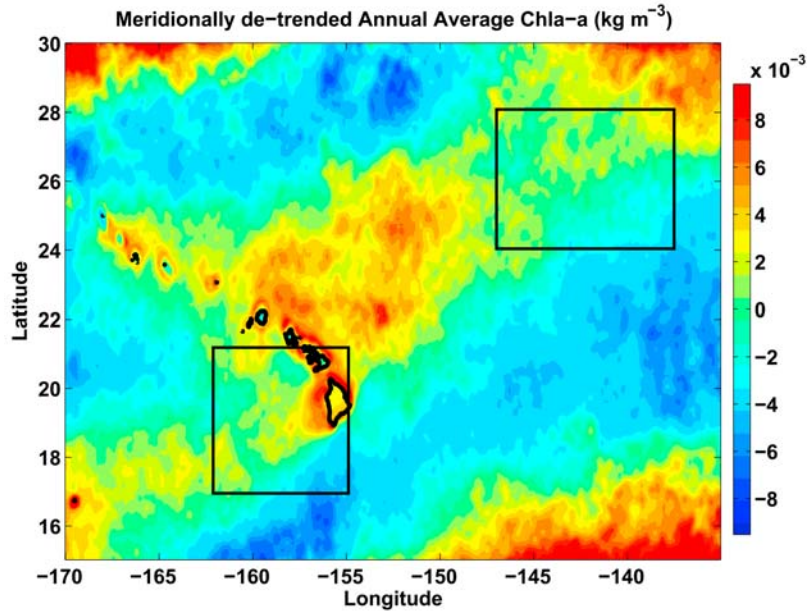

Figure 8. Average surface chlorophyll-a from 2003 to 2007 meridionally detrended by removing a linear fit at each longitude. The average slope was 0.028 kg m^{-3} km^{-1}.

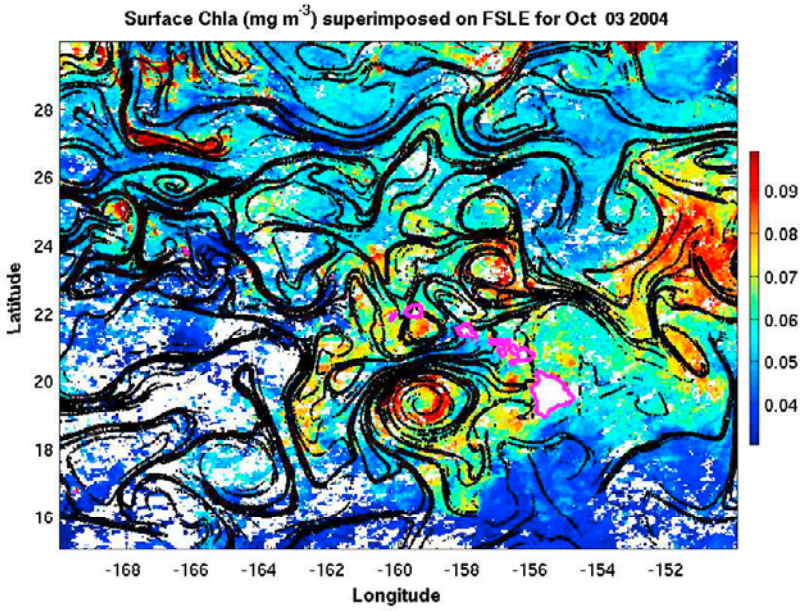

Figure 9. Large (top 20%) values of FSLE calculated for 3 October 2004 superimposed on surface chlorophyll-a for the same period. Note the general agreement between the unstable manifolds and the chlorophyll-a patches (see text for details).

0.32 and in the case of EKE, it is 0.27. Although low, both values were substantially larger than the correlation obtained with the absolute chlorophyll-a average (both values are significant at the 95% confidence level). The reason for that is probably because of the clearer signal, after detrending, in the immediate lee of the island of Hawaii, which is not easily seen in the averaged values.

[31] The detrended annual mean surface chlorophyll-a shows elevated values in the vicinity of the Hawaiian islands. Interestingly, the region of high chlorophyll-a that extends, approximately, 1000 km to the northeast of the islands is contained within the region of elevated FSLE, with their northeastern limit approximately coinciding.

[32] The other interesting region is the tongue of high chlorophyll-a trailing off to the south west of the Big Island toward Johnston Atoll (at 16.8°N, 169°W). Although not showing up distinctly in the annual mean as a tongue, there is often a pattern of high FSLE in this region. As we will see in the next section, the modeling study shows this region to be one of strong stretching and strong vertical motions.

3.2. Unstable Manifolds, Transport Barriers, and Frontogenesis

[33] Unstable manifolds have been shown to shape and control the evolution of tracer distribution in the surface ocean on synoptic scales [*Lehahn et al.*, 2007]. The calculation of the backward FSLE's from satellite-derived geostrophic velocities for the broader region around the Hawaiian islands for 3 October 2004 (Figure 9) shows that the same applies in this oligotrophic region, where a tendency for the patches to be stirred along, rather than across, these transport barriers is observed.

[34] To understand the effect of the straining of the geostrophic field on the surface distribution of chlorophyll-a for the two regions shown in the previous section, we calculate the FSLE for the same periods as in Figures 2–5. Contours of the largest values of the backward FSLE's are superimposed on the surface temperature anomalies and chlorophyll-a concentration for 3 October 2004, for the region in the lee of the islands, and 24 August 2004, for the region northeast of the islands, and shown in Figure 10. These dates were chosen because they correspond to the periods when the chlorophyll-a patch is most intense in each case.

[35] The visual agreement between the chlorophyll-a patches, the surface temperature fronts and the largest backward FSLE is clear. Large values of λ are seen at the edges of the anticyclone centered at 159.5° (Figures 10a and 10b), where the chlorophyll-a concentration is also large. The time variability of the flow creates spiraling isolines of λ within the strong anticyclone, which allows the horizontal exchange of ambient waters with the inner region of the eddy along the unstable manifolds [*Lehahn et al.*, 2007].

[36] With regard to the region northeast of the islands, the same agreement between the FSLE's and the surface chlorophyll-a patches is observed, even though the mesoscale eddy and stirring fields are substantially weaker in this region when compared to the lee of the islands (see Figures 1 and 6). Maximum values of λ in this region were, approximately, 0.15 day^{-1} as opposed to, approximately, 0.2 day^{-1} in the lee of the islands.

[37] Previous studies [cf. *Lehahn et al.*, 2007] have shown a strong relationship between satellite derived FSLE and ocean color. A noticeable difference between this and previous studies is that in our case the chlorophyll-a streaks appear not to be a consequence of the stirring of an initially larger patch. Instead, the appearance and persistence for two or three weeks of submesoscale streaks strongly suggests that local mechanisms of vertical injection of nutrients are at play in these regions of large straining and relative vorticity gradients. Once nutrients are injected into the surface ocean at these transient upwelling hot spots, horizontal stirring

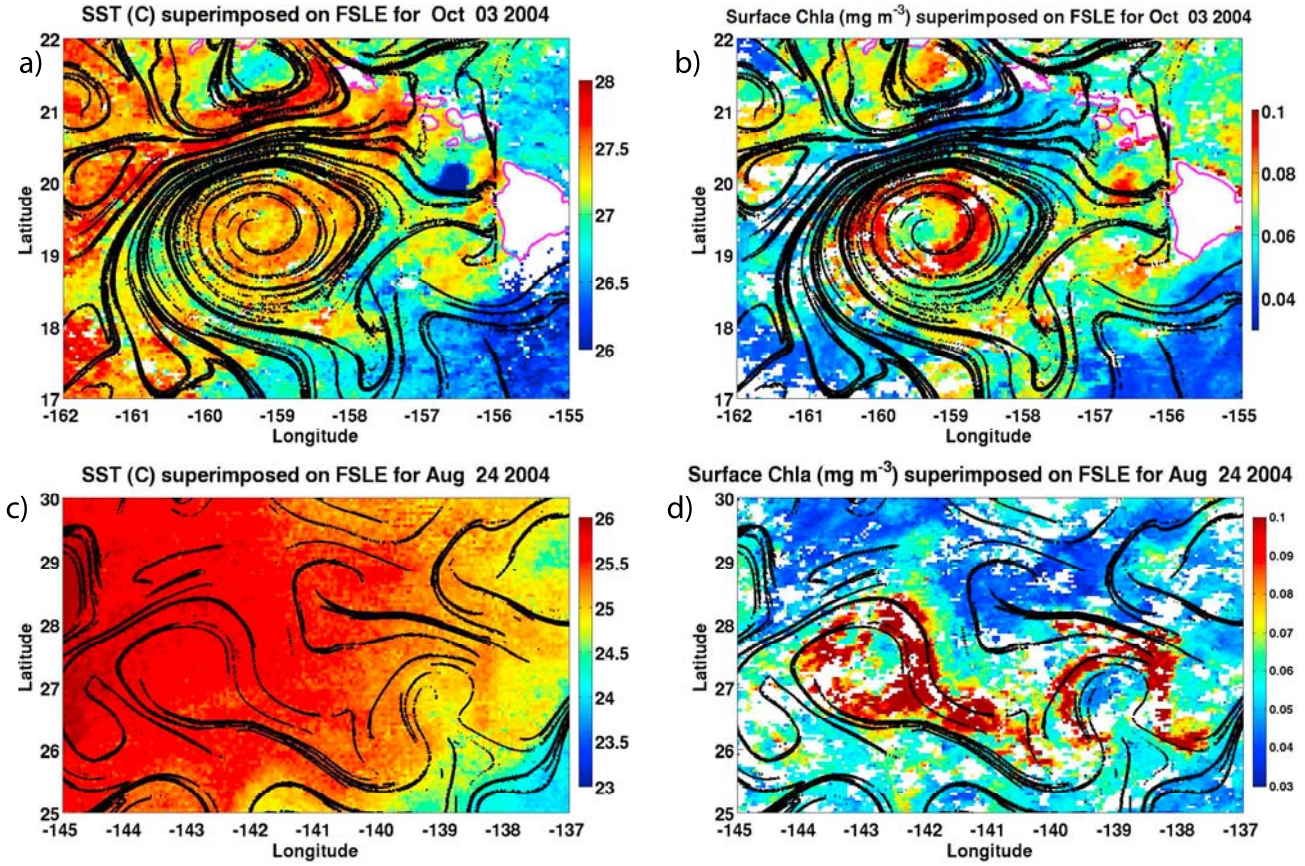

Figure 10. Large values (top 20%) of backward FSLEs (black lines) superimposed on (a) SST and (b) chlorophyll-a on 3 October 2004 in the lee of Hawaii. Large values (top 20%) of backward FSLEs superimposed on (c) SST and (d) chlorophyll-a on 24 August 2004 northeast of the islands. Maximum values of λ were approximately 0.15 day^{-1} northeast of the islands and approximately 0.2 day^{-1} in the lee of the islands.

then shapes the unstable manifolds, which control the evolution of the tracer distribution.

[38] Despite the good agreement in these particular examples, large values of λ do not necessarily imply large chlorophyll-a concentrations at the surface nor are the they necessarily coincident with SST fronts, as can be seen in the western part of Figure 9 for the case of chlorophyll-a concentration. We must keep in mind that there are other processes at play that do not necessarily depend on the horizontal stretching of the flow field (i.e., eddy pumping, air-sea interaction, buoyancy forcing). Also, the time history of biogeochemical elements, the depth of the induced overturning cells relative to the nutricline and the tendency for frontogenesis to restratify the surface ocean [cf. *Lapeyre et al.*, 2006], all contribute to the signal in ocean color.

4. Model Estimates

[39] The observations show that high chlorophyll-a concentrations occur within regions of large strain associated with surface temperature fronts. The localized intensification of the patches suggest local mechanisms of vertical injection. Unfortunately, there are no subsurface observations that could help clarify the origin of the biomass. Therefore we turn to a numerical model.

4.1. Model Configuration

[40] Because of computational restrictions, we performed model simulations focusing on the lee of the Hawaiian islands using the Regional Ocean Modeling System (ROMS) [*Shchepetkin and McWilliams*, 2005]. Partial submesoscale resolution was achieved with a 2 km horizontal resolution grid. There are 30 vertical layers, with the stretching parameters of the s coordinates chosen to give high vertical resolution in the upper 200 m. There are four open boundaries along which 10 day averages are taken from a climatological run from Estimating the Circulation and Climate of the Ocean (ECCO) [*Stammer et al.*, 1999]. The K profile parameterization (KPP) was employed for vertical mixing [*Large et al.*, 1994]. The model domain ranges from 164.5°W to 153.5°W and from 16°N to 22.5°N. The model is spun up for 2 years and the results presented in this paper correspond to 2 day averages of the month of October of the third year model run.

[41] Temporal and spatial resolution of the wind stress have been shown to substantially affect the regional circulation [*Calil et al.*, 2008]. The monthly QuikSCAT climatology used here captures the wind stress curl intensification in the lee of the islands [cf. *Calil et al.*, 2008] and a realistic EKE pattern is reproduced in the region of interest (Figure 11).

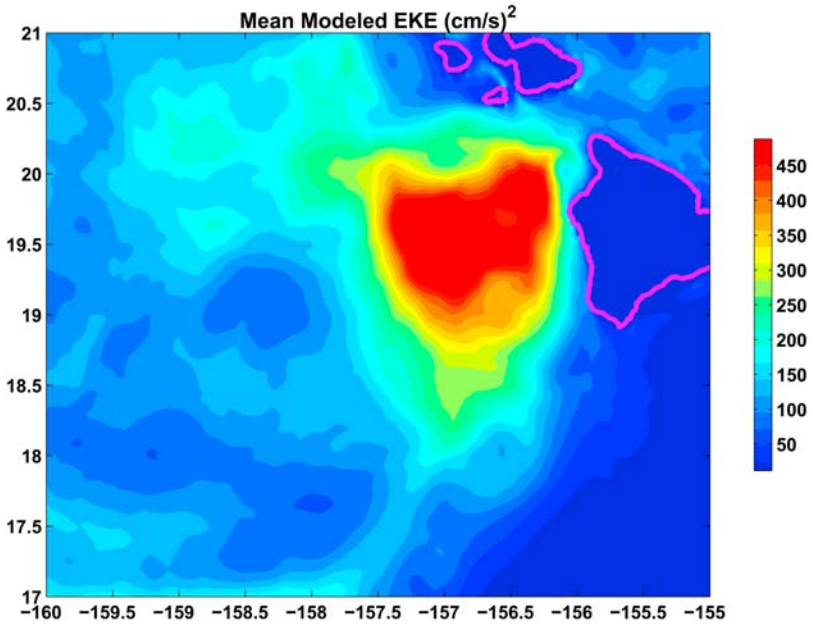

Figure 11. Modeled eddy kinetic energy ((cm/s)^2) calculated from sea surface height anomalies for the third year of model run.

[42] The time variability of the wind forcing is also important in generating EKE, which is underestimated when a monthly climatology is used. Nevertheless, for the purposes of this study we consider this product appropriate as a lower limit of the importance of the wind forcing. Higher temporal and spatial resolution of the wind will certainly yield larger values of EKE and Ekman pumping (see section 4.4). Given the observational motivation, in this section we will focus on model vertical velocities associated with surface density fronts, relative vorticity gradients and regions of large strain in the lee of the islands, away from the model boundaries.

4.2. Model Results: FSLE and the Vertical Velocity Field

[43] The subsurface Rossby number at 10 m obtained from a 2 day average model output (Figure 12 (top)) shows strong meso- and submesoscale vortices and filaments with O(1) Ro in the lee of the islands. Filaments and the edges of mesoscale eddies are also characterized by large horizontal density gradients (Figure 12 (bottom)), large strain and large vertical velocities (Figure 13 (top)), with maximum values exceeding 60 m d^{-1} at 50 m depth (Figure 14).

[44] Narrow strips of large vertical velocities are associated with the edges of the strong anticyclone just west of the island of Hawaii. The same does not occur with the cyclonic eddy located to the northwest, where a broader and weaker structure is observed in the vertical velocity field.

[45] The density field shows the intrusion of lighter fluid from the west into the lee while heavier fluid flows from the east just south of the island of Hawaii. The encounter of these two bodies of water creates a weak surface density front which is enhanced by the action of the geostrophic deformation field.

[46] Superimposed on the surface potential density, in Figure 12 (bottom), are the largest backward FSLE's, with values between 0.15 and 0.3 day^{-1}, obtained using model horizontal velocities at z = −60 m. As in the observations, they tend to coincide with regions of density gradients, such as surface fronts and the edges of mesoscale eddies, where the model simulation exhibits large vertical velocities. Hence, our model results suggest a clear connection between regions of large straining and the generation of large vertical velocities.

[47] As mentioned earlier, in regions where the frontal intensification is largest, the thermal wind imbalance gives rise to ageostrophic secondary circulations (ASC's), which will act to restore the balance by restratifying the surface ocean. Vertical velocities are generated in order to readjust the vertical shear of the horizontal velocity to the thermal wind. Figure 14 shows a meridional transect of w at 158.58°W, across the density front, that illustrates this situation. Much of this pattern is in agreement with what would be expected from frontogenesis. Downwelling (≈60 m d^{-1}) occurs on the heavy side of the front, and upwelling (≈20 m d^{-1}) on the light side. Upwelling is associated with negative relative vorticity and downwelling with positive relative vorticity. There is a tendency for restratification (i.e., to flatten the isopycnals), in a manner consistent with previous studies of surface ocean frontogenesis [*Lapeyre and Klein*, 2006].

[48] Many processes can generate vertical velocities in the ocean and their importance might vary under different conditions [*Giordani et al.*, 2006]. Given the characteristics of the evolution of the chlorophyll patches shown in section 2 (i.e., their tendency to be coincident with the edges of mesoscale features and weak surface temperature fronts) and the robustness of the trade winds in the region around Hawaii, two processes arise as fundamentally important in generating vertical velocities in the region, surface frontogenesis and NLEP. We now proceed to isolate, with the model data, these two processes and compare them with the model vertical velocity.

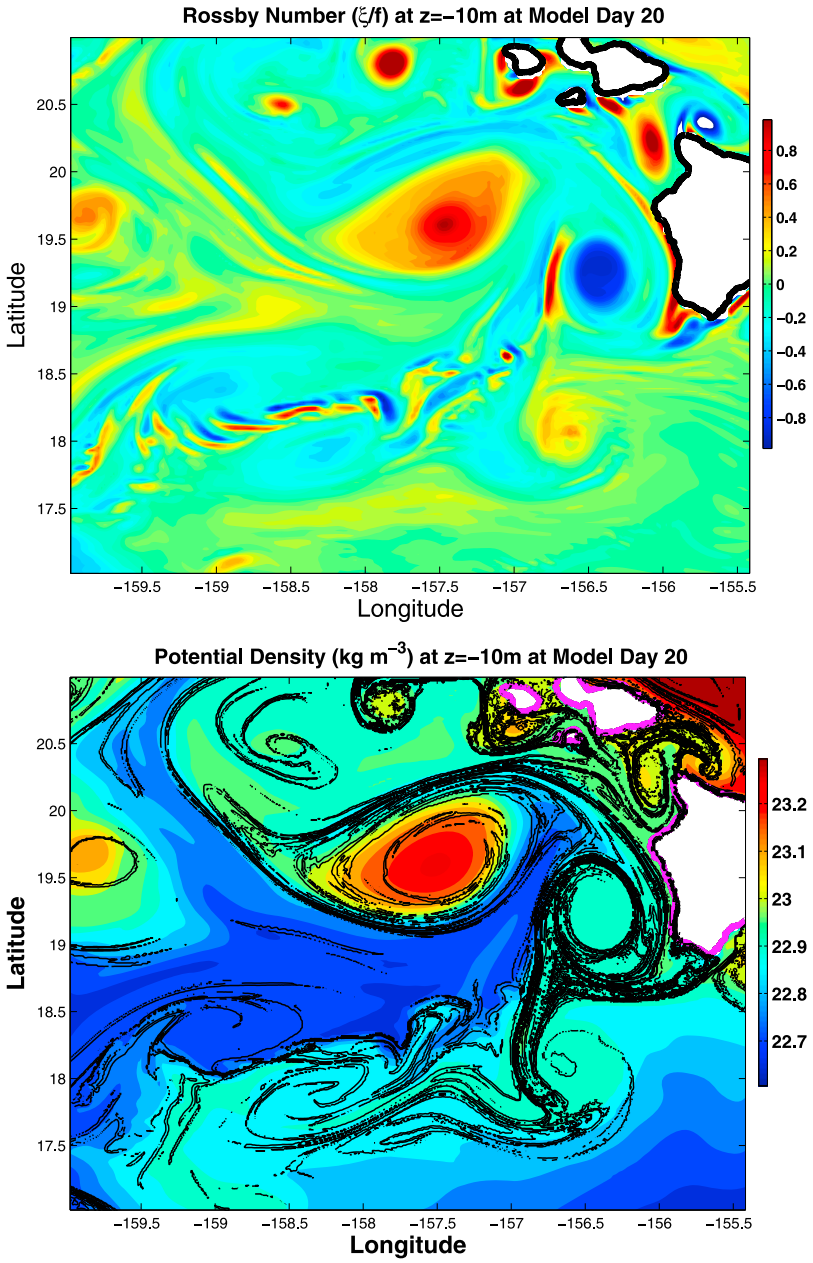

Figure 12. Two day average of (top) Rossby number and (bottom) FSLEs superimposed on potential density field at 10 m depth for model day 20 of the run.

4.3. Diagnosis of Strain-Driven Frontogenesis

[49] One way to qualitatively diagnose ageostrophic vertical motion due to frontogenesis is by means of the Q vector form of the omega equation [*Hoskins et al.*, 1978]

$$N^2\nabla_h^2 w + f_0^2\frac{\partial^2 w}{\partial z^2} = 2\nabla\cdot\mathbf{Q}, \tag{2}$$

where N is the buoyancy frequency, w the vertical velocity and $\mathbf{Q}$ is the Q vector, defined as

$$\mathbf{Q} = \frac{g}{\rho_0}\left(\frac{\partial \mathbf{v_g}}{\partial x}\cdot\nabla\rho', \frac{\partial \mathbf{v_g}}{\partial y}\cdot\nabla\rho'\right), \tag{3}$$

where ρ' is the potential density anomaly and $\mathbf{v_g} = (u_g, v_g)$, the horizontal geostrophic velocity.

[50] We make use of the Q vector merely as an indicator of where vertical motion might occur as a consequence of the deformation the geostrophic field imposes on the density field, causing an imbalance in the thermal wind which must be restored by the ASC's. The Q vector form of the omega equation has proven successful in estimating vertical velocities from field observations and model results. In the traditional omega equation, the cancellation between the differential vorticity advection and density advection causes problems in estimating w correctly [*Fiekas et al.*, 1994; *Strass*, 1994; *Pollard and Regier*, 1992; *Tintoré et al.*, 1991]. Rather than solving equation (3) to obtain w, we note the relationship between w and $\nabla\cdot\mathbf{Q}$. If w has a

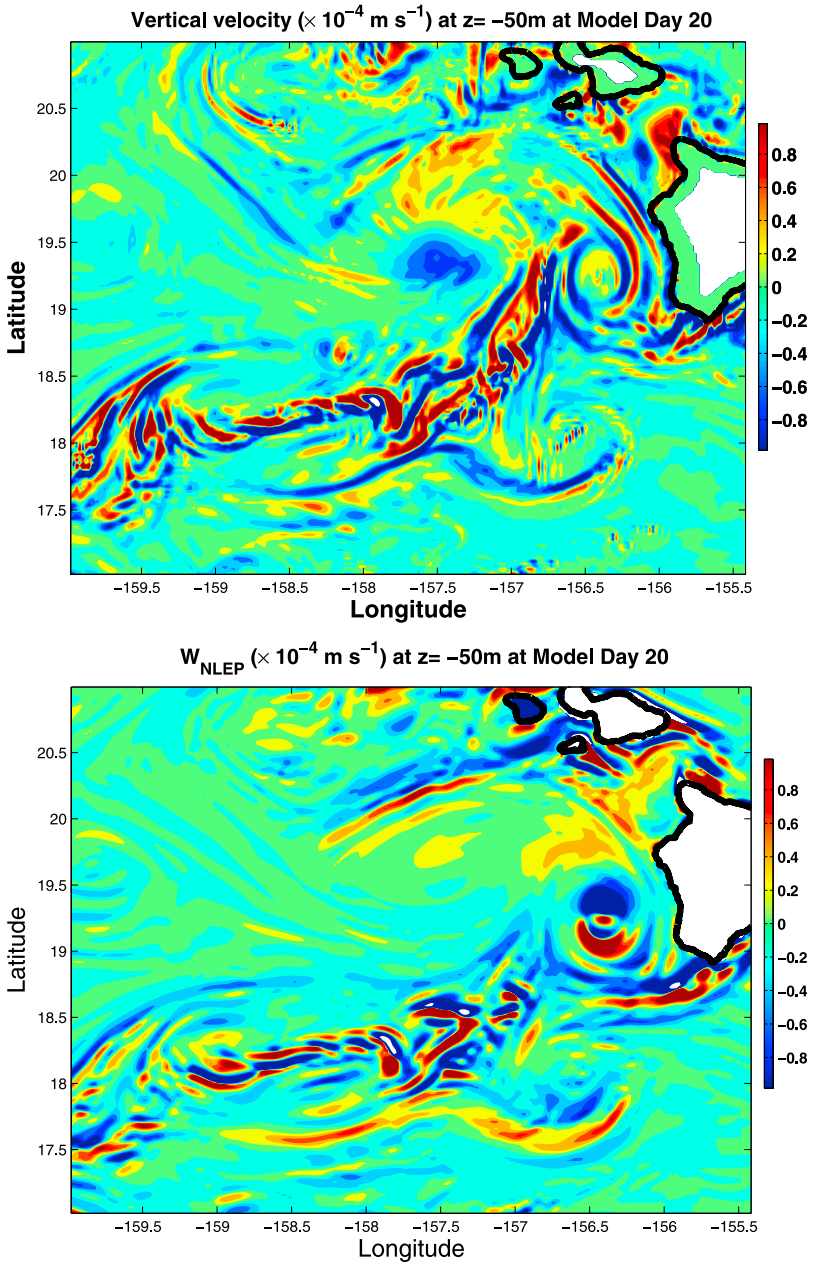

Figure 13. (top) Horizontal slice of 2 day averaged model vertical velocities on model day 20 at z = −50 m. (bottom) Nonlinear Ekman pumping calculated for the same period.

sinusoidal behavior in equation (2), upward motion is indicated by the convergence of the Q vector [*Hoskins et al.*, 1978].

[51] A point-by-point correlation between w and $\nabla \cdot \mathbf{Q}$ is found to vary with time and location. Here we focus on the region in the vicinity of the density front and the two mesoscale eddies. A subregion of the model (see Figure 16) was used to avoid the land mask and regions near the boundaries while retaining the regions where vertical component of velocity is largest. The density front is most unstable, based on the intensity of the vertical velocities and the appearance of submesoscale vorticity ripples, on model day 20. To reduce noise, the fields were smoothed by a moving average of three grid points. The Q vector was calculated at depths 10−60 m. The average of the upper 60 m, where the ASC's are most intense, is presented here. The comparison was made at various time steps during the run, with consistently similar results. A scatter plot of the 60 m averaged vertical velocity and $\nabla \cdot \mathbf{Q}$ for model day 20 is shown in Figure 15. There is a clear inverse relationship between $\nabla \cdot \mathbf{Q}$ and w. A linear fit was used to estimate the slope in the linear fit between $\nabla \cdot \mathbf{Q}$ and w at each time step. For this month the slope was, on average, 1.1×10^{-12} $(\mathrm{ms})^2$.

[52] We define $w_{\nabla \cdot \mathbf{Q}} = \alpha \nabla \cdot \mathbf{Q}$, where α is the slope of the linear fit between w and $\nabla \cdot \mathbf{Q}$, i.e., $w_{\nabla \cdot \mathbf{Q}}$ is an estimate of w based solely on the Q vector. Figures 16 (top) and 16 (bottom) shows w and $w_{\nabla \cdot \mathbf{Q}}$, respectively, calculated for the same time (day 20) as that of Figure 12 and for the region over which the fit was calculated. There is

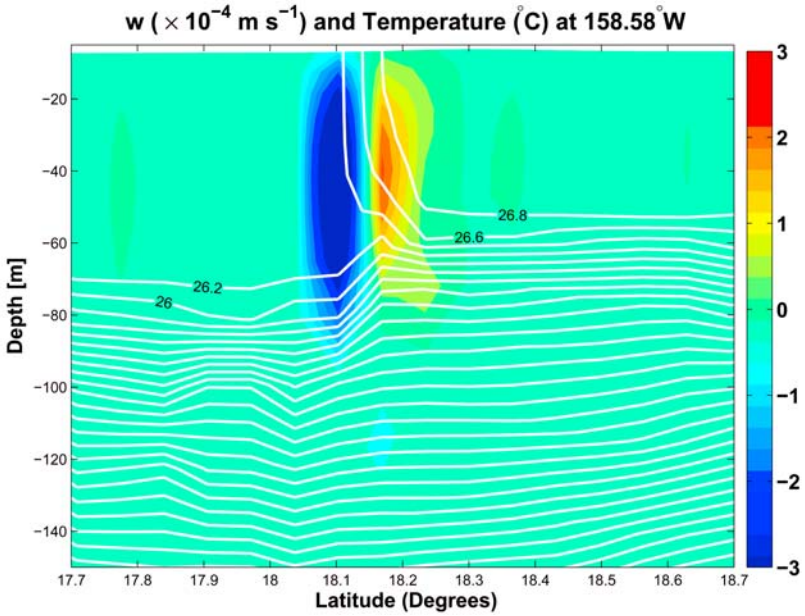

Figure 14. Meridional transect of model vertical velocity and potential temperature between 17.7°N and 18.7°N at 158.58°W. Model time is the same as in Figure 12.

remarkable agreement in the region of strongest w, with $w_{\nabla \cdot \mathbf{Q}}$ capturing most of the spatial pattern of w. This strongly suggests that large vertical velocities are associated with strong straining and possibly frontogenesis.

[53] The submesoscale alternating pattern of w at the edges of the anticyclone centered at 156.5°W is partially reproduced by $w_{\nabla \cdot \mathbf{Q}}$, in particular where vertical velocities and horizontal density gradients are most intense (i.e., its northwestern edge).

[54] In the vicinity of the cyclonic eddy centered at, approximately, 157.5°W, where w is weak (see Figure 12), $w_{\nabla \cdot \mathbf{Q}}$ overestimates the amplitude but again captures the basic pattern of w. The overestimation is not unexpected as the same fit of w and $w_{\nabla \cdot \mathbf{Q}}$ will not necessarily apply across the whole domain. The results do suggest, however, that if used with caution $w_{\nabla \cdot \mathbf{Q}}$ provides a good estimate of the spatial patterns of w.

[55] The point-by-point correlation coefficient between w and $\nabla \cdot \mathbf{Q}$ varied with time (Figure 17). The values

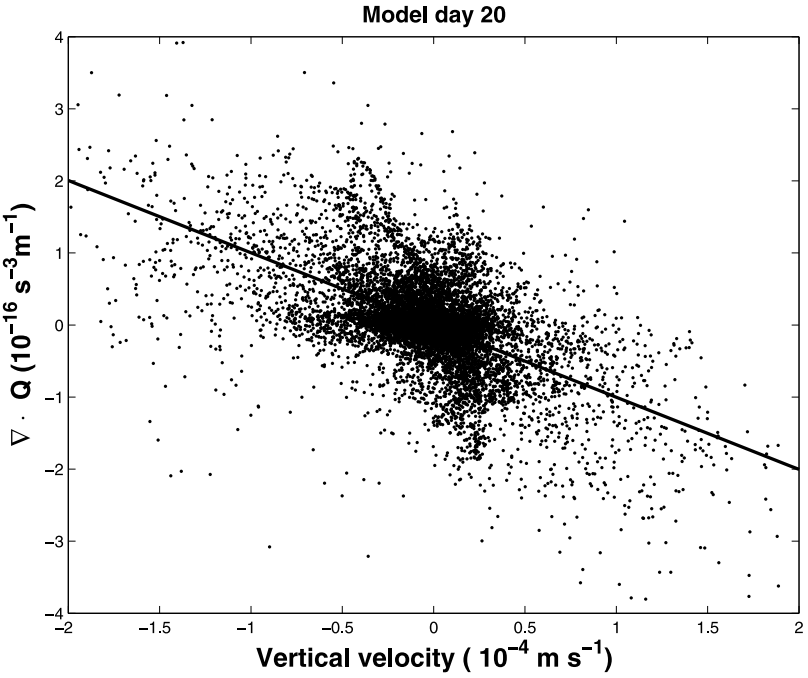

Figure 15. An example of a scatterplot of the 60 m average of $\nabla \cdot Q$ and w, with the correspondent linear fit superimposed for model day 20.

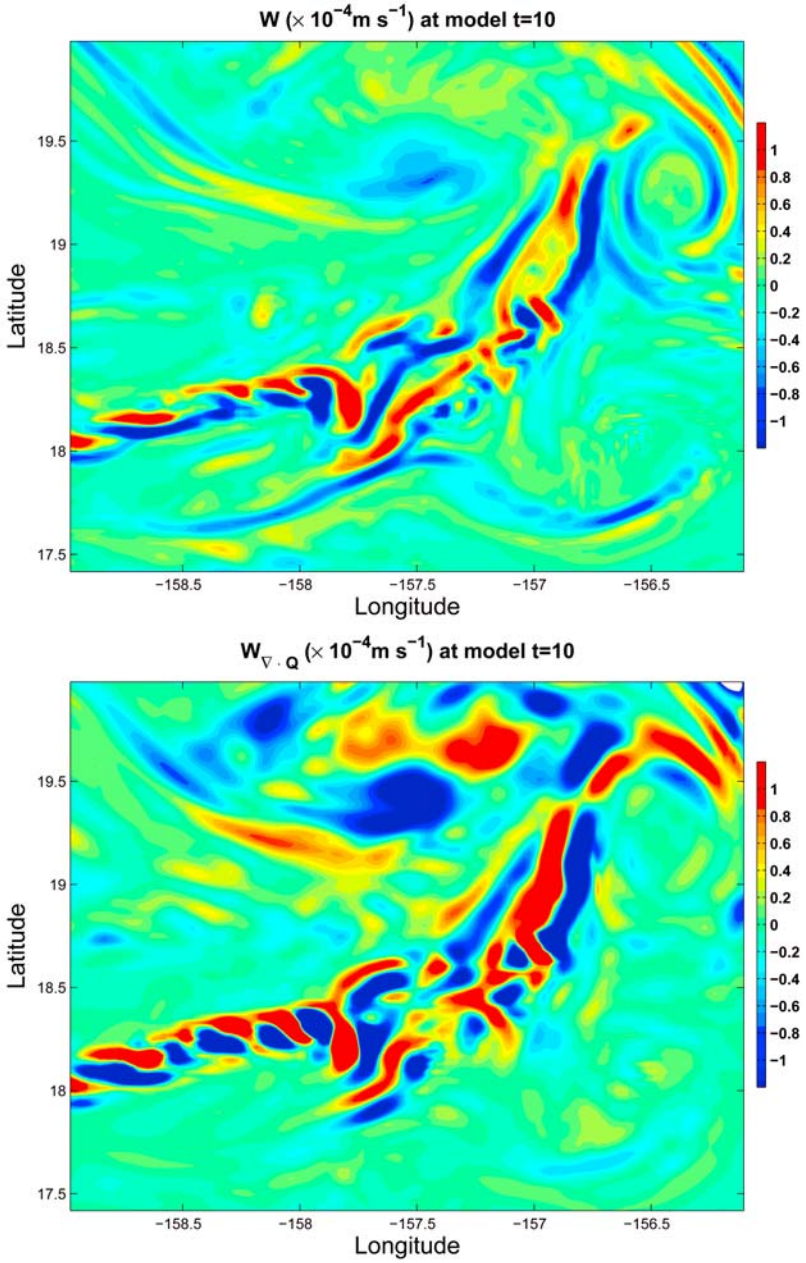

Figure 16. (top) Model vertical velocity averaged in the upper 60 m on model day 20, and (bottom) $w_{\nabla \cdot \mathbf{Q}}$ obtained by multiplying $\nabla \cdot \mathbf{Q}$ by the slope of the linear fit.

ranged between 0.3 and, approximately, 0.6, and were larger when the density front and vertical velocities were larger (days 16–20). All values are statistically significant at the 95% confidence.

[56] The fact that the correlation between w and $w_{\nabla \cdot \mathbf{Q}}$ is larger during the most intense phase of front instability is consistent with the study of *Wang and Ikeda* [1997] that diagnosed the vertical velocity by solving the Q vector omega equation within an unstable baroclinic wave. Their results showed a better agreement during the developing phase of the baroclinic wave than during the decaying phase.

[57] One characteristic of intense frontal motions is the generation of significant cyclonic vorticity intermittency [*Klein et al.*, 2008; *Capet et al.*, 2008; *Garnier et al.*, 1998; *Wang*, 1993; *Klein and Hua*, 1988]. At frontal scales, O(1) Rossby number requires the inclusion of the relative vorticty in the stretching term of the vorticity balance, which creates a positive feedback favoring cyclonic vorticity. Intermittency is characterized by long tails in the probability density function (PDF), resembling an exponential law.

[58] The PDF for the relative vorticity normalized by the planetary vorticity from the 2 day average output for one year of our model run is shown in Figure 18 (top) for three different depths, z = 20 m, z = 50 m and z = 200 m. The asymmetry between the cyclonic and anticyclonic vorticity is clear. Long tails in the cyclonic vorticity, following an exponential law, are clearly observed in the upper layer. On the anticyclonic side, the values decay faster with Ro at a

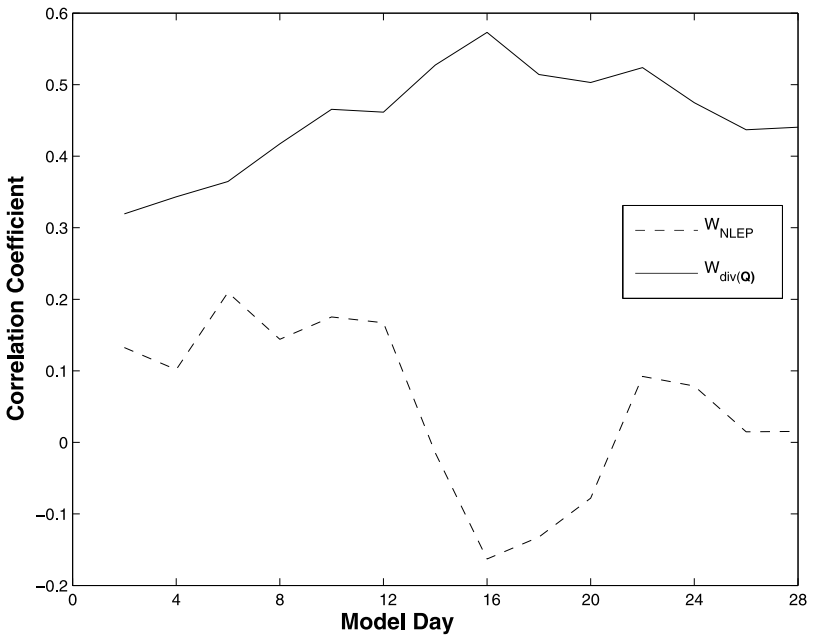

Figure 17. Time series of the point-by-point correlation coefficient between $w_{\nabla \cdot \mathbf{Q}}$ and w (solid line) and w_{NLEP} and w(dashed line).

rate resembling, although not exactly, a Gaussian distribution. One explanation for that might be the fact that strong, coherent anticyclones are formed and propagate through the region. The "bump" observed at high negative Ro is a consequence of strong, coherent anticyclones that are formed in the southern part of the lee of Hawaii. In open ocean flows such a pattern is not expected [*Capet et al.*, 2008; *Klein et al.*, 2008]. At z = 200 m, as expected, the PDF is much more symmetrical.

[59] Although our simulation does not fully resolve the submesoscale, the asymmetry in relative vorticity is a consequence of the increased horizontal resolution of the model. For comparison, the PDF, for the same region, of 4 years of a 8 km resolution run forced with QuikSCAT daily winds for the year 2005 [cf. *Calil et al.*, 2008] is shown in Figure 18 (bottom). The distribution of cyclonic vorticity falls off much faster than in the 2 km resolution run shown in Figure 18 (top). Note that the increased resolution does not affect substantially the anticyclonic side of the PDF. Except for the peak observed at, approximately, $Ro = -1.2$ in the 2 km PDF, which shows that anticyclonic eddies are stronger in the high-resolution run, the distributions are relatively similar, as opposed to the cyclonic side. This is further evidence that the non-Gaussian behavior of the anticyclonic side of the PDF is because of the robust anticyclonic eddies formed in the lee of the Hawaii.

[60] One way to quantify intermittency is to calculate the kurtosis (Ku) of a random variable, the ratio of the fourth-order moment to the square of the variance. The higher the value of kurtosis, the more important extreme, sporadic events are in the variance of a random variable. For a Gaussian distribution Ku is equal to 3. Values of Ku are shown in Table 1.

[61] Values of Ku decrease from the surface to 200 m. At 20 m, Ku is 8.32, which is still low compared to values near 40 obtained by *Klein et al.* [2008], but substantially larger than 3, showing that the vorticity distribution is not Gaussian. Instead, it is characterized by narrow regions with large gradients. At higher resolutions, these asymmetries are expected to be larger [*Capet et al.*, 2008].

[62] The PDF for the vertical velocities (Figure 19) did not yield such a strong asymmetry, although downwelling velocities were consistently larger than upwelling velocities, which can also be seen in the skewness values in Table 1. This suggests that the 2 km resolution may not be enough to fully resolve all aspects of the submesoscale dynamics.

4.4. Nonlinear Ekman Pumping

[63] In regions of intense wind stress and relatively strong horizontal current gradients (e.g., at the edges of mesoscale features), Ekman-induced vertical velocities will be generated not only by the curl of the wind stress but also by the interaction of the surface wind stress with the vertical component of the geostrophic relative vorticity [*Thomas and Rhines*, 2002; *Hart*, 1996; *Lee et al.*, 1994; *Stern*, 1965]. The leading order term of the NLEP is

$$w_{nl} = \frac{1}{\rho}\hat{z} \cdot \nabla \times \frac{\boldsymbol{\tau}}{f + \xi_g}, \tag{4}$$

where $\boldsymbol{\tau}$ is the surface wind stress and ξ_g is the geostrophic relative vorticity. Note that a uniform wind induces vertical velocities where the geostrophic relative vorticity is spatially varying.

[64] The sparse resolution of the satellite altimetry product (in our case, approximately 30 km) does not allow an accurate calculation of the gradient of the geostrophic relative vorticity, but a simple estimate can be made using typical values. Suppose a zonal wind stress of 0.1 N/m^2, not uncommon in the region, blows over a front with a relative vorticity of 10^{-5} s^{-1} varying within a spatial scale of

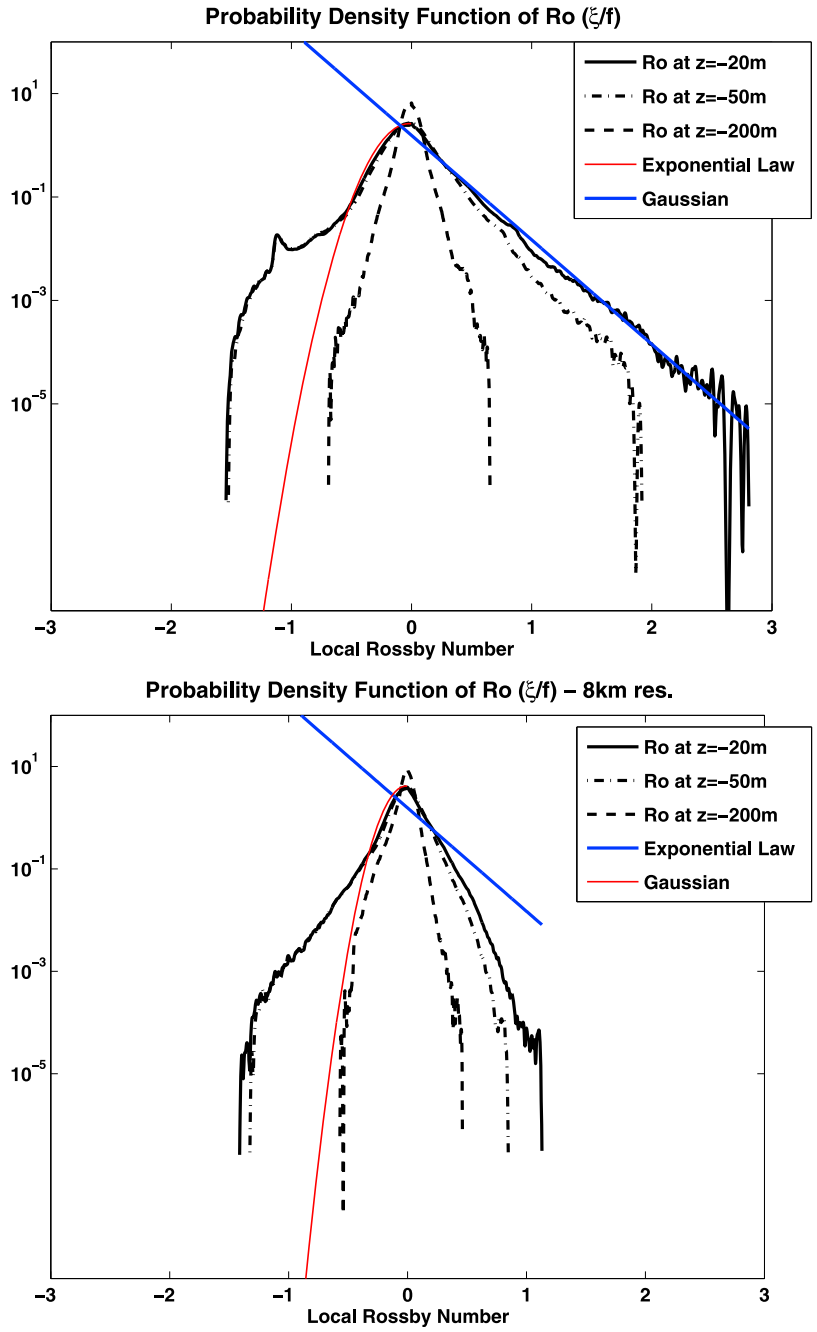

Figure 18. (top) Probability density function of the Rossby number ($\frac{\xi}{f}$) for 1 year of simulation for a region between 157°W and 162°W and 17.5°N and 20°N in the model domain. The Gaussian distribution (red) has the same mean and standard deviation as Ro at 20 m. Exponential law is plotted in blue. (bottom) Probability density function of the Rossby number ($\frac{\xi}{f}$) for 4 years of simulation at 8 km resolution for a region between 157°W and 167°W and 17.5°N and 20°N in the model domain. The Gaussian distribution (red) has the same mean and standard deviation as Ro at 20 m. For comparison, exponential law (blue) is the same as in Figure 18 (top).

10 km. Then equation (4) yields a NLEP velocity of 5 m/d in the case of preexisting anticyclonic relative vorticity and 2.5 m/d for cyclonic vorticity. On smaller scales the values of both the wind stress and the relative vorticity gradients can be much larger. On moderate wind conditions NLEP will be more intense at the edges of the vortices where the gradients of ξ are large, while in their cores it will be smaller because of the roughly solid body rotation.

[65] In the case of our simulations, the daily temporal and spatial variations of the wind field are not included in the monthly wind product. Hence, our values constitute a lower limit for NLEP. Because of large intensity and small-scale wind stress curl, daily winds would yield even larger NLEP values.

[66] NLEP (w_{NLEP}) was calculated via equation (4), using the horizontal geostrophic velocities from the model at

Table 1. Kurtosis and Skewness of the Rossby Number and Vertical Velocities[a]

	Rossby Number ($\frac{\zeta}{f}$)			Vertical Velocity		
Property	20 m	50 m	200	20 m	50 m	200 m
Kurtosis	8.32	8.11	5.49	18.41	23.06	14.19
Skewness	0.51	−0.18	0.04	−1.17	−0.69	0.03

[a]From Figures 18 and 19.

different depths. A horizontal slice at 50 m depth is shown in Figure 13 (bottom). In general, the spatial structure of w_{NLEP} and w is very similar with the two being of a similar magnitude. In the region of the cyclonic eddy previously mentioned w_{NLEP} is smaller than w, which is expected based on the fact that it will be diminished(enhanced) in regions of cyclonic(anticyclonic) vorticity.

[67] Within the anticyclonic eddy, w_{NLEP} is much larger than the model vertical velocities. The largest term of w_{NLEP} in this case is the one associated with the zonal wind stress, which is much larger than its meridional counterpart, and the meridional gradient of relative vorticity. Since this term is inversely proportional to the square of the absolute vorticity, it will be larger where anticyclonic vorticity is larger (i.e., more negative), which will tend to overshadow the component generated by the gradients of relative vorticity at the edges of the eddy. At the density front, the largest values are in anticyclonic regions where the gradients of relative vorticity are large.

[68] A point-by-point correlation between the depth-integrated w_{NLEP} and w in the upper 60 m is much smaller than in the case of $w_{\nabla \cdot \mathbf{Q}}$ (see Figure 17, dashed line), and is indeed negative at times when the front is at its strongest. This poor correlation suggests that nonlinear Ekman pumping is not the only mechanism at play and that the phase relationship may be destroyed by other processes. The strong similarity between much of the structure seen in Figure 13 does strongly suggest, however, that nonlinear Ekman pumping is playing a significant role in the upper ocean dynamics.

5. Discussion and Concluding Remarks

[69] In this paper we have explored the formation of chlorophyll-a patches associated with regions of large straining and surface temperature fronts in the subtropical, oligotrophic ocean in the vicinity of the Hawaiian islands. Two case studies in regions with contrasting levels of EKE show the strong relationship between SST, ocean color, and the occurrence of strong stretching characterized by the FSLE.

[70] A large correlation between the FSLE's and EKE was found in the region as a whole, supporting previous studies which showed that horizontal stirring can be estimated through EKE [*Waugh and Abraham*, 2008; *Waugh et al.*, 2006]. For the relatively low EKE values of the Hawaiian region, a linear fit is a good approximation for the relationship.

[71] The meridionally detrended chlorophyll-a average also shows a tail of higher values to the west-southwest of the island chain. The region coincides with the propagation path of the anticyclones that form in the region. It is left for future studies to investigate the importance of the anticyclonic lee eddies in creating this feature.

[72] We have also studied the effect of the intensification of surface fronts caused by the geostrophic deformation field, their interaction with the local wind stress, the subsequent generation of large vertical velocities at submesoscales that may cause episodic nutrient injections that

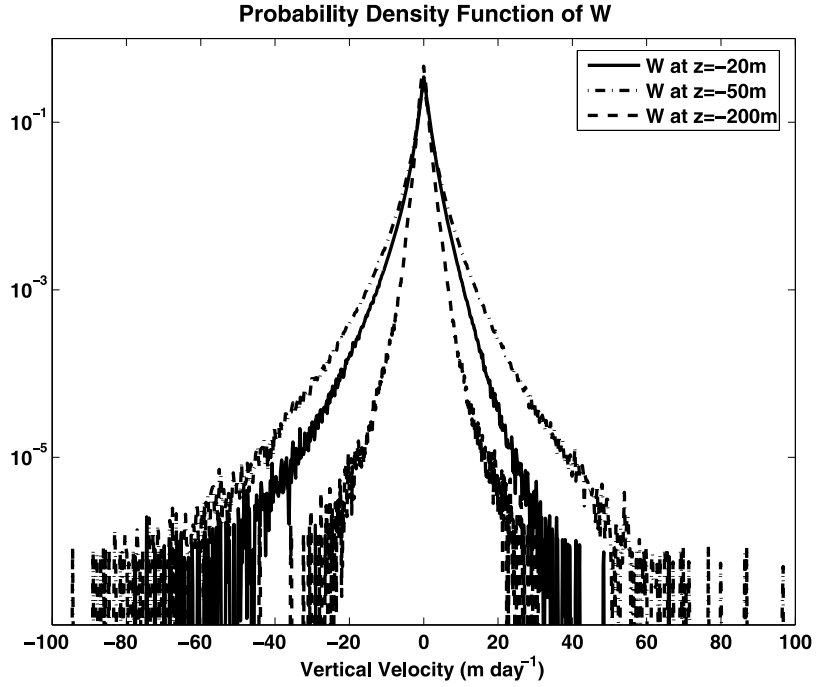

Figure 19. Probability density function of the vertical velocity for 1 year of high-resolution simulation for a region between 157°W and 162°W and 17.5°N and 20°N in the model domain.

result in streaky chlorophyll-a patches observed in the region.

[73] The intermittency of these motions, their ubiquity and the large values of vertical velocities make these processes potentially important agents in maintaining regional new production rates. In fact, previous studies that included submesoscale filamentary processes have shown a substantial increase in the vertical flux of tracers and primary productivity [*Lapeyre and Klein*, 2006; *Lévy et al.*, 2001; *Mahadevan and Archer*, 2000]. Because of their transient nature, these processes are relatively independent of the remineralization time scale of isopycnals (i.e., the likelihood of these isopycnals to have been recently uplifted, hence ineffective for new production, is rather small), one of the criticisms about the efficiency of the mesoscale eddy-pumping mechanism [*Martin and Pondaven*, 2003; *Oschlies*, 2002].

[74] We speculate that the impact on the ecosystem of the surface-intensified submesoscale vertical motions will be greatest under severe nutrient limitation and shallow mixed layer depth (MLD). The MLD is shallower during summertime. From monthly cruises at Station ALOHA (22°45′N, 158°00′W), the estimated average MLD in the summer is, approximately, 40 m (the average MLD for the 20 year long time series is around 64 m). Hence, ASC's would be able to reach the upper part of the pycnocline, facilitating the vertical supply of nutrients located at the top of the nutricline, especially during summer. Submesoscale processes, thus, are a potential explanation for a more effective physical supply of nutrients during summertime, which might play a role in the development of the late summer surface chlorophyll-a blooms frequently observed around Station ALOHA [*Dore et al.*, 2008], as indicated in Figures 4 and 5. The persistence of the observed chlorophyll-a patches shown in this study strongly suggests that local nutrient injection is occurring in these narrow regions, since in the oligotrophic ocean nutrients that are made available at the surface are rapidly consumed in the absence of additional supply.

[75] The modeling study of *Calil et al.* [2008], in the lee of Hawaii, has shown that there is a tendency for filamentation in regions between mesoscale features associated with large strain and vorticity gradients [*Calil et al.*, 2008]. Given the regional characteristics of circulation and forcing, we believe that surface frontogenesis and NLEP are the most relevant processes in generating large vertical velocities at frontal scales.

[76] The model simulations used in this study show that vertical velocities generated by these two processes (order of tens of meters per day) are much larger than those usually associated with mesoscale processes (e.g., uplifting of isopycnals during cyclone formation).

[77] The simple diagnostic used in this study to estimate frontogenetically generated vertical velocities showed a good correlation with the modeled vertical velocity in the upper ocean, despite the large spatial variability. NLEP seems, according to our results, to be less directly related, on a point-by-point comparison, to the vertical velocity field, although the similar spatial structure and magnitude suggest that NLEP is an important process in the upper ocean dynamics.

[78] These two processes, although different in nature, are related in the sense that regions of large strain are, often times, regions of large gradient in relative vorticity and O(1) Ro. It is known, however, that they do not necessarily act in conjunction. Ekman velocities are dependent on the direction of the wind, and may augment or oppose the frontogenetically generated upwelling [*Capet et al.*, 2008].

[79] The fact that these vertical motions are associated with regions of horizontal stirring has implications for primary productivity. *Martin et al.* [2002] investigated the effect of localized upwelling on primary production. They determined that large vertical transport associated with intense horizontal mixing between upwelling and ambient waters significantly increase biological productivity.

[80] We have shown, in the case of the observed features, that chlorophyll-a patches tend to be horizontally stirred along the unstable manifolds. In our model simulations, we have shown that regions of large stirring are coincident with regions of large submesoscale vertical velocities. Thus, these processes provide the connection between the vertical input of nutrients at the submesoscales and their horizontal redistribution in nutrient-limited waters, fulfilling the preconditions for increased patchy productivity as hypothesized by *Martin et al.* [2002].

[81] These submesoscale physical processes might also affect biological processes (i.e., N_2 fixation) that alleviate the nutrient limitation in the region [*Karl et al.*, 1997]. The interplay between the biological and physical forcing in the supply of nutrients in this oligotrophic region has not been fully explored as yet.

[82] Given that the Hawaiian region is characterized by the robust northeasterly trade winds and by a vigorous mesoscale eddy field, both NLEP and surface frontogenesis are clearly important for the generation of large vertical velocities and provide a possible explanation for the observed surface chlorophyll-a patchiness with potential impact on primary and export production.

[83] **Acknowledgments.** The authors would like to thank Eric Firing and two anonymous reviewers for careful and insightful comments which substantially improved the initial manuscript. Thanks are also due to Francesco D'Ovidio for providing the FSLE routines. P.H.R. Calil gratefully acknowledges support from the Coordenaç ao de Aperfeiçoamento de Pessoal de Nível Superior (CAPES), Brazilian Ministry of Education, through a Ph.D. scholarship (process 1526-02-2). Additional funding was provided by the Maui High Performance Computing Center (MHPCC) through an Engagement grant (2007) and the Center for Microbial Oceanography: Research and Education (CMORE). Numerical simulations used in this study were performed at MHPCC's Hurricane, an IBM cluster that retired in 2008.

References

Artale, V., G. Boffetta, A. Celani, M. Cencini, and A. Vulpiani (1997), Dispersion of passive tracers in closed basins: Beyond the diffusion coefficient, *Phys. Fluids*, *9*, 3162–3171.

Aurell, E., G. Boffetta, A. Crisanti, G. Paladin, and A. Vulpiani (1997), Predictability in the large: an extension of the concept of Lyapunov exponent, *J. Phys. A Math. Gen.*, *30*, 1–26.

Calil, P. H. R., K. J. Richards, Y. Jia, and R. R. Bidigare (2008), Eddy activity in the lee of the Hawaiian islands, *Deep Sea Res. Part II*, *55*(10–13), 1179–1194, doi:10.1016/j.dsr2.2008.01.008.

Capet, X., J. McWilliams, M. Molemaker, and A. Shchepetkin (2008), Mesoscale to submesoscale transition in the California Current System. Part I: Flow structure, eddy flux, and observational tests, *J. Phys. Oceanogr.*, *38*(1), 29–43.

Dore, J., R. Letelier, M. Church, R. Lukas, and D. Karl (2008), Summer phytoplankton blooms in the oligotrophic North Pacific Subtropical Gyre: Historical perspective and recent observations, *Prog. Oceanogr.*, *76*(1), 2–38.

d'Ovidio, F., V. Fernandez, E. Hernandez-Garca, and C. Lopez (2004), Mixing structures in the Mediterranean Sea from finite-size

Lyapunov exponents, *Geophys. Res. Lett.*, *31*, L17203, doi:10.1029/2004GL020328.
d'Ovidio, F., J. Isern-Fontanet, C. López, E. Hernández-García, and E. García-Ladona (2009), Comparison between Eulerian diagnostics and finite-size Lyapunov exponents computed from altimetry in the Algerian basin, *Deep Sea Res. Part I*, *56*(1), 15–31.
Falkowski, P., D. Ziemann, Z. Kolber, and P. Bienfang (1991), Role of eddy pumping in enhancing primary production in the ocean, *Nature*, *352*, 55–58.
Fiekas, V., H. Leach, K. Mirbach, and J. Woods (1994), Mesoscale instability and upwelling. Part 1: Observations at the North Atlantic Intergyre Front, *J. Phys. Oceanogr.*, *24*(8), 1750–1758.
Flament, P., R. Lumpkin, J. Tournadre, and L. Armi (2001), Vortex pairing in an unstable anticyclonic shear flow: Discrete subharmonics of one pendulum day, *J. Fluid Mech.*, *440*, 401–409.
Garnier, E., O. Métais, and M. Lesieur (1998), Synoptic and frontal-cyclone scale instabilities in baroclinic jet flows, *J. Atmos. Sci.*, *55*(8), 1316–1335.
Giordani, H., L. Prieur, and G. Caniaux (2006), Advanced insights into sources of vertical velocity in the ocean, *Ocean Dyn.*, *56*(5), 513–524.
Hakim, G., C. Snyder, and D. Muraki (2002), A new surface model for cyclone–anticyclone asymmetry, *J. Atmos. Sci.*, *59*(16), 2405–2420.
Hart, J. (1996), On nonlinear Ekman surface-layer pumping, *J. Phys. Oceanogr.*, *26*(7), 1370–1374.
Hoskins, B. J. (1982), The mathematical theory of frontogenesis, *Annu. Rev. Fluid Mech.*, *14*(1), 131–151, doi:10.1146/annurev.fl.14.010182.001023.
Hoskins, B. J., and F. Bretherton (1972), Atmospheric frontogenesis models: Mathematical formulation and solution, *J. Atmos. Sci.*, *29*(1), 11–37.
Hoskins, B. J., I. Draghici, and H. Davies (1978), A new look at the ω-equation, *Quart. J. R. Meteor. Soc.*, *104*, 31–38.
Karl, D., R. Letelier, L. Tupas, J. Dore, J. Christian, and D. Hebel (1997), The role of nitrogen fixation in biogeochemical cycling in the subtropical North Pacific Ocean, *Nature*, *388*(6642), 533–538.
Klein, P., and B. Hua (1988), Mesoscale heterogeneity of the wind-driven mixed layer: Influence of a quasigeostrophic flow, *J. Mar. Res.*, *46*(3), 495–525.
Klein, P., B. Hua, G. Lapeyre, X. Capet, S. Le Gentil, and H. Sasaki (2008), Upper ocean turbulence from high-resolution 3D simulations, *J. Phys. Oceanogr.*, *38*(8), 1748–1763.
Kuwahara, V., F. Nencioli, T. Dickey, Y. Rii, and R. Bidigare (2008), Physical dynamics and biological implications of Cyclone Noah in the lee of Hawai'i during E-Flux I, *Deep Sea Res. Part II*, *55*(10–13), 1231–1251.
Lapeyre, G., and P. Klein (2006), Impact of small-scale filaments on the oceanic vertical pump, *J. Mar. Res.*, *64*, 835–851.
Lapeyre, G., P. Klein, and B. Hua (2006), Oceanic restratification forced by surface frontogenesis, *J. Phys. Oceanogr.*, *36*(8), 1577–1590.
Large, W. G., J. C. McWilliams, and S. C. Doney (1994), Oceanic vertical mixing: A review and a model with nonlocal boundary layer parameterization, *Rev. Geophys.*, *32*, 363–403.
Lee, D., P. Niiler, A. Warn-Varnas, and S. Piacsek (1994), Wind-driven secondary circulation in ocean mesoscale, *J. Mar. Res.*, *52*(3), 371–396.
Legal, C., P. Klein, A. Treguier, and J. Paillet (2007), Diagnosis of the vertical motions in a mesoscale stirring region, *J. Phys. Oceanogr.*, *37*(5), 1413–1424.
Lehahn, Y., F. d'Ovidio, M. Lévy, and E. Heifetz (2007), Stirring of the northeast Atlantic spring bloom: A Lagrangian analysis based on multi-satellite data, *J. Geophys. Res.*, *112*, C08005, doi:10.1029/2006JC003927.
Lévy, M., P. Klein, and A. M. Treguier (2001), Impact of sub-mesoscale physics on production and subduction of phytoplankton inan oligotrophic regime, *J. Mar. Res.*, *59*, 535–565.
Lumpkin, C. F. (1998), Eddies and currents in the Hawaiian islands, Ph.D. thesis, 282 pp., Sch. of Ocean and Earth Sci. and Technol., Univ. of Hawaii at Manoa, Honolulu.
Mahadevan, A., and D. Archer (2000), Modeling the impact of fronts and mesoscale circulation on the nutrient supply and biogeochemistry of the upper ocean, *J. Geophys. Res.*, *105*(C1), 1209–1226.
Mahadevan, A., and A. Tandon (2006), An analysis of mechanisms for submesoscale vertical motion at ocean fronts, *Ocean Modell.*, *14*, 241–256.
Mahadevan, A., L. N. Thomas, and A. Tandon (2008), Comment on "Eddy/wind interactions stimulate extraordinary mid-ocean plankton blooms," *Science*, *320*(5875), 448, doi:10.1126/science1152111.
Martin, A. P., and P. Pondaven (2003), On estimates for the vertical nitrate flux due to eddy pumping, *J. Geophys. Res.*, *108*(C11), 3359, doi:10.1029/2003JC001841.
Martin, A. P., and K. Richards (2001), Mechanisms for vertical transport within a north atlantic mesoscale eddy, *Deep Sea Res. Part II*, *48*, 757–773.
Martin, A. P., K. Richards, A. Bracco, and A. Provenzale (2002), Patchy productivity in the open ocean, *Global Biogeochem. Cycles*, *16*(2), 1025, doi:10.1029/2001GB001449.
McGillicuddy, D. J., Jr., and A. R. Robinson (1997), Eddy-induced nutrient supply and new production in the Sargasso Sea, *Deep Sea Res. Part II*, *44*, 1427–1450.
McGillicuddy, D. J., Jr., A. R. Robinson, D. Siegel, H. Jannasch, R. Johnson, T. Dickey, J. McNeil, A. Michaels, and A. Knap (1998), Influence of mesoscale eddies on new production in the Sargasso Sea, *Nature*, *394*, 263–265.
McGillicuddy, D. J., Jr., et al. (2007), Eddy/wind interactions stimulate extraordinary mid-ocean plankton blooms, *Science*, *316*(5827), 1021–1026, doi:10.1126/science.1136256.
McGillicuddy, D. J., Jr., J. R. Ledwell, and L. A. Anderson (2008), Response to Comment on "Eddy/wind interactions stimulate extraordinary mid-ocean plankton blooms," *Science*, *320*(5875), 448, doi:10.1126/science.1148974.
Nencioli, F., V. Kuwahara, T. Dickey, Y. Rii, and R. Bidigare (2008), Physical dynamics and biological implications of a mesoscale eddy in the lee of Hawai'i: Cyclone Opal observations during E-Flux III, *Deep Sea Res. Part II*, *55*, 1252–1274.
Oschlies, A. (2002), Can eddies make ocean deserts bloom?, *Global Biogeochem. Cycles*, *16*(4), 1106, doi:10.1029/2001GB001830.
Pollard, R. T., and L. A. Regier (1992), Vorticity and vertical circulation at an ocean front, *J. Phys. Oceanogr.*, *22*(6), 609–625.
Shchepetkin, A., and J. C. McWilliams (2005), The regional oceanic modelling system (ROMS): A split-explicit, free-surface, topography-following-coordinate oceanic model, *Ocean Modell.*, *9*, 347–404.
Stammer, D., et al. (1999), The consortium for estimating the circulation and climate of the ocean (ECCO)—Science goals and task plan, *Rep. 1*, Estim. the Circ. and Clim. of the Ocean Consortium, Cambridge, Mass.
Stern, M. (1965), Interaction of a uniform wind stress with a geostrophic vortex, *Deep Sea Res.*, *12*, 355–367.
Strass, V. (1994), Mesoscale instability and upwelling. Part 2: Testing the diagnostics of vertical motion with a three-dimensional ocean front model, *J. Phys. Oceanogr.*, *24*(8), 1759–1767.
Thomas, L., and C. Lee (2005), Intensification of ocean fronts by down-front winds, *J. Phys. Oceanogr.*, *35*(6), 1086–1102.
Thomas, L., and P. Rhines (2002), Nonlinear stratified spin-up, *J. Fluid Mech.*, *473*, 211–244.
Tintoré, J., D. Gomis, S. Alonso, and G. Parrilla (1991), Mesoscale dynamics and vertical motion in the Alborán Sea, *J. Phys. Oceanogr.*, *21*(6), 811–823.
Wang, D. (1993), Model of frontogenesis: Subduction and upwelling, *J. Mar. Res.*, *51*(3), 497–513.
Wang, J., and M. Ikeda (1997), Diagnosing ocean unstable baroclinic waves and meanders using the quasigeostrophic equations and Q vector method, *J. Phys. Oceanogr.*, *27*(6), 1158–1172.
Waugh, D., and E. Abraham (2008), Stirring in the global surface ocean, *Geophys. Res. Lett.*, *35*, L20605, doi:10.1029/2008GL035526.
Waugh, D., E. Abraham, and M. Bowen (2006), Spatial variations of stirring in the surface ocean: A case study of the Tasman Sea, *J. Phys. Oceanogr.*, *36*(3), 526–542.
Williams, R., and M. Follows (2003), Physical transport of nutrients and the maintenance of biological production, in *Ocean Biogeochemistry: The Role of the Ocean Carbon Cycle in Global Change*, edited by R. Zahn et al., pp. 19–51, Springer, Berlin.
Wilson, C. (2003), Late summer chlorophyll blooms in the oligotrophic North Pacific Subtropical Gyre, *Geophys. Res. Lett.*, *30*(18), 1942, doi:10.1029/2003GL017770.

P. H. R. Calil and K. J. Richards, Department of Oceanography, University of Hawaii at Manoa, 1000 Pope Rd., Marine Sciences Bldg. 205, Honolulu, HI 96822, USA. (calil@hawaii.edu)